

TABLE 1
 ABELL/ACO CLUSTERS OBSERVED IN 10° SQUARE CENTERED ON AQUARIUS SUPERCLUSTER

Cluster	α J2000	δ J2000	Velocity km s ⁻¹	Error km s ⁻¹	Emission Reference
2523	23:03:04.08	-16:50:06.4	9138	89	
	23:03:16.24	-17:14:36.0	37928	75	
	23:03:35.41	-17:04:20.8	37026	73	
	23:03:37.31	-17:08:49.2	38898	96	
	23:03:52.07	-17:16:25.4	22188	73	
	23:04:28.21	-17:16:14.4	38213	52	
	23:05:14.63	-17:02:35.3	15677	51	
	23:05:28.57	-17:08:00.3	19278	77	
2547	23:10:28.45	-20:54:10.3	19469	71	
	23:10:31.42	-21:06:21.4	44396	55	
	23:10:46.61	-21:07:57.9	44723	35	
	23:10:57.77	-21:11:34.0	44898	35	
	23:11:16.04	-21:09:45.4	15820	89	
	23:11:32.76	-20:48:39.1	19278	92	
	23:12:01.73	-20:58:06.3	26771	27	
	23:12:35.03	-20:55:05.1	19181	23	
2548	23:13:03.26	-20:55:57.6	4351	63	
	23:09:51.00	-20:47:50.1	24723	96	
	23:10:27.35	-20:44:08.7	26407	28	
	23:10:53.04	-20:25:37.2	24183	35	
	23:11:01.55	-20:32:33.1	33249	41	
	23:11:03.26	-20:22:20.7	17581	86	
	23:11:12.26	-20:43:39.2	31575	29	
	23:11:15.77	-20:25:05.2	33151	26	
	23:11:40.55	-20:26:10.3	33107	26	
	23:11:58.45	-20:21:25.5	26337	24	
	23:12:09.18	-20:37:01.3	26289	20	
	23:12:13.27	-20:47:49.2	26499	22	
2553	23:12:22.74	-20:24:44.4	15873	50	
	23:12:54.88	-20:43:03.0	24966	22	
	23:10:13.22	-24:45:12.0	33287	47	
	23:10:14.02	-24:48:36.5	33072	21	
	23:10:18.88	-25:10:58.8	43363	39	
	23:10:23.40	-25:01:27.7	34677	22	
	23:10:46.54	-24:43:52.8	34857	60	
	23:11:05.37	-25:05:20.2	44181	75	
	23:11:32.80	-25:12:53.8	14941	86	
	23:11:38.33	-24:54:22.0	26211	26	
	23:11:44.01	-24:50:31.3	44129	65	
	23:11:51.82	-25:12:39.7	9502	32	
23:11:52.73	-24:47:00.9	34740	27		
23:11:58.13	-24:32:30.6	22865	62		
23:12:25.96	-25:00:31.5	34821	27		
23:12:38.34	-24:48:41.4	15414	83		
23:12:44.49	-24:44:09.2	14655	40		
23:13:02.31	-25:03:21.7	34500	44		
23:13:07.31	-25:07:33.1	43830	52		

TABLE 1—*Continued*

Cluster	α J2000	δ J2000	Velocity km s ⁻¹	Error km s ⁻¹	Emission Reference
2555	23:14:11.47	-25:07:12.0	24176	28	
	23:11:45.76	-22:05:55.4	32867	34	
	23:11:49.62	-22:21:37.4	9411	86	
	23:12:32.74	-22:12:31.0	33159	48	
	23:12:49.17	-22:10:18.0	41874	92	
	23:12:51.15	-22:15:26.1	33316	28	
	23:13:49.84	-22:05:16.3	50530	60	
2556	23:14:20.02	-22:01:00.2	47183	41	
	23:11:24.35	-21:39:23.3	45903	51	
	23:11:35.73	-21:44:46.7	36447	30	
	23:11:37.99	-21:51:58.0	19165	27	
	23:12:04.75	-21:29:17.5	32134	26	
	23:12:13.27	-21:39:56.6	32837	60	
	23:12:19.88	-21:30:09.1	32589	32	
	23:12:29.84	-21:39:23.6	26272	40	
	23:12:36.15	-21:50:35.6	41727	27	
	23:12:47.19	-21:35:40.7	26095	33	
	23:13:01.36	-21:38:03.3	26460	29	
	23:13:19.56	-21:41:55.1	26198	59	
	23:14:14.43	-21:45:12.8	33372	28	
2557	23:11:18.32	-16:50:31.6	37651	40	
	23:11:37.97	-16:44:48.9	28751	62	
	23:11:46.95	-17:09:00.7	53669	56	
	23:12:09.26	-17:20:05.7	41448	51	
	23:12:22.49	-17:10:44.3	35369	25	
	23:12:47.44	-16:41:31.2	19699	96	2a
	23:12:53.05	-17:02:46.8	51874	63	
	23:13:00.92	-17:00:08.1	52077	49	
	23:13:09.53	-16:55:39.3	28170	48	1a
	23:13:21.97	-17:05:06.6	41163	71	
	23:13:27.67	-16:52:50.8	50471	60	
	23:13:45.26	-17:07:01.8	49907	62	
	23:13:51.19	-16:50:14.4	32271	25	
	23:13:58.74	-16:43:44.1	37675	44	
	23:14:24.91	-17:10:39.2	23693	53	
23:14:26.85	-17:06:22.9	27449	24		
23:14:43.50	-16:48:51.8	32367	53		
23:14:45.28	-17:18:15.0	51919	47		
2579	23:19:28.89	-21:22:57.1	25593	50	
	23:19:41.26	-21:28:55.5	25280	28	
	23:19:41.42	-21:32:43.7	25128	48	
	23:20:07.17	-21:35:45.4	9369	80	
	23:20:19.95	-21:46:14.4	25208	31	
	23:20:34.65	-21:34:39.0	33249	77	
	23:20:50.38	-21:29:19.4	42424	41	
23:21:15.37	-21:35:06.1	32918	39		
23:21:16.43	-21:17:21.3	9230	28		

TABLE 1—*Continued*

Cluster	α J2000	δ J2000	Velocity km s ⁻¹	Error km s ⁻¹	Emission Reference
	23:21:26.61	-21:29:06.0	33587	41	
	23:21:27.21	-21:56:52.3	24092	96	
	23:21:50.38	-21:29:08.4	33050	31	
	23:22:12.10	-21:30:58.8	33831	49	
	23:22:24.08	-21:26:51.8	18556	24	
	23:22:49.59	-21:38:29.6	35322	62	
2585	23:21:09.27	-26:15:14.3	8370	25	5a
	23:21:18.63	-26:30:25.4	32524	27	
	23:21:27.72	-26:00:19.0	54115	59	
	23:21:41.14	-26:31:31.2	21422	89	6a
	23:21:48.96	-26:20:22.5	57724	75	
	23:22:14.31	-26:07:47.5	13818	36	4a
	23:22:37.37	-26:02:55.9	33708	23	
	23:22:45.86	-25:57:36.0	26912	50	3a
	23:22:52.54	-26:21:18.5	56905	20	7e
	23:23:03.18	-26:13:16.4	57523	73	
	23:23:07.52	-25:53:13.5	46018	80	
	23:24:07.65	-26:07:06.6	56440	80	
2599	23:24:41.88	-26:05:11.6	25968	26	
	23:24:48.25	-23:35:38.5	20149	33	
	23:25:14.84	-23:35:02.9	26506	26	
	23:25:21.58	-23:44:05.7	63812	59	14a
	23:25:29.12	-24:05:19.4	33348	26	
	23:25:55.73	-23:30:49.9	25916	86	12a
	23:26:14.20	-24:06:30.3	33414	22	
	23:26:30.17	-23:56:19.4	27055	38	13a
	23:26:34.78	-23:25:12.3	18710	32	
	23:26:38.15	-23:46:03.3	37724	26	
	23:26:41.35	-23:51:13.2	26395	23	
	23:26:45.33	-23:27:11.1	18889	29	
	23:26:46.95	-23:57:51.9	32743	21	
	23:26:57.15	-23:35:59.8	33158	20	11e
	23:27:10.28	-23:44:29.8	37099	39	
	23:27:12.65	-24:07:48.3	34150	41	
	23:27:14.77	-23:50:40.5	26899	53	
	23:27:21.18	-23:29:57.8	1709	20	10e
	23:27:45.24	-24:00:00.6	26972	28	8a
	23:28:25.17	-23:52:34.8	34500	24	
	23:28:31.94	-23:33:36.1	34155	35	
	23:28:33.75	-23:47:31.0	26697	60	9a
2600	23:24:51.59	-22:33:48.3	36861	25	
	23:25:00.86	-22:12:46.8	34504	22	24a
	23:25:07.71	-22:25:09.3	36826	31	
	23:25:41.33	-22:07:52.2	35371	25	22a
	23:25:52.18	-22:13:29.3	35566	24	23a
	23:26:02.59	-22:22:59.0	34616	32	25a
	23:26:06.35	-22:05:44.6	10308	96	21a

TABLE 1—*Continued*

Cluster	α J2000	δ J2000	Velocity km s ⁻¹	Error km s ⁻¹	Emission Reference
	23:26:36.10	-22:26:55.0	36890	30	26e
	23:26:17.52	-21:59:07.5	18587	31	20a
	23:26:22.69	-22:24:33.2	17670	29	
	23:26:27.56	-22:43:23.9	26356	21	
	23:26:29.23	-22:05:59.8	18771	20	
	23:26:44.87	-22:06:15.0	18119	24	19a
	23:26:48.50	-22:31:24.0	36605	65	27a
	23:27:00.42	-22:26:08.8	33343	22	
	23:27:08.20	-22:23:34.5	26462	21	
	23:27:15.41	-22:18:43.7	18053	60	18a
	23:27:32.35	-22:19:29.4	36039	29	
	23:27:40.97	-22:25:49.7	18139	38	17a
	23:27:41.49	-21:58:52.1	37432	41	
	23:28:03.91	-22:31:37.7	26107	17	16a
	23:28:21.76	-22:41:11.4	38604	30	
	23:28:32.87	-22:30:25.5	18646	27	15a
2601	23:25:01.67	-24:18:11.1	2765	20	29e
	23:25:09.81	-24:29:02.6	20360	40	30a
	23:25:12.69	-24:38:14.5	26285	22	
	23:25:13.56	-24:23:39.4	14817	48	
	23:25:29.12	-24:05:19.4	33312	31	
	23:26:14.20	-24:06:30.3	33395	22	
	23:26:14.97	-24:16:19.6	37842	20	28e
	23:26:47.34	-24:06:16.5	33225	44	
	23:27:04.57	-24:26:05.2	31687	24	
	23:27:23.17	-24:34:00.5	63683	62	
	23:27:29.29	-24:18:22.8	34176	71	
	23:27:38.89	-24:39:33.9	33696	21	
	23:28:15.81	-24:03:08.7	46552	62	
	23:28:24.19	-24:22:26.0	34012	32	
	23:28:38.69	-24:33:24.4	22200	86	
2608	23:29:22.34	-21:28:33.7	15797	34	
	23:29:25.64	-21:39:25.0	14091	46	33a
	23:29:55.27	-21:48:48.8	15620	49	
	23:30:10.72	-21:33:56.6	48754	53	
	23:30:16.67	-22:04:04.5	40473	32	
	23:30:38.00	-21:41:55.8	47073	50	
	23:30:50.79	-21:49:12.4	31434	25	
	23:30:59.80	-21:24:21.7	14560	55	
	23:31:07.84	-21:27:28.8	14569	44	
	23:31:15.99	-21:55:45.2	31337	29	
	23:31:17.67	-21:32:08.7	45895	52	
	23:31:28.30	-21:55:17.6	31308	23	
	23:31:34.16	-21:50:03.5	35613	31	31a
	23:32:04.93	-21:40:45.9	31282	42	
	23:32:14.41	-21:26:44.6	19574	38	32a
2609	23:28:43.49	-26:13:58.9	33110	51	

TABLE 1—*Continued*

Cluster	α J2000	δ J2000	Velocity km s ⁻¹	Error km s ⁻¹	Emission Reference
	23:28:59.60	-26:01:07.9	32965	39	37a
	23:29:17.07	-26:13:37.1	41264	60	
	23:29:19.39	-25:48:12.9	32869	28	
	23:29:21.17	-26:16:33.1	29787	65	
	23:29:21.52	-26:04:59.6	41159	41	
	23:29:46.57	-26:22:01.1	32831	24	
	23:29:49.10	-25:44:58.5	38384	77	
	23:29:55.37	-26:24:19.1	24372	26	
	23:30:14.90	-26:04:52.5	63277	20	36e
	23:30:25.49	-25:57:15.3	8372	44	
	23:30:27.44	-26:13:06.9	25548	30	38e
	23:30:28.64	-25:43:45.3	26819	48	
	23:30:42.43	-26:09:00.0	42372	38	
	23:30:53.95	-26:09:20.6	41409	47	
	23:30:54.69	-26:01:34.4	26886	22	35a
	23:30:55.19	-25:52:10.5	58412	89	
	23:31:16.29	-26:03:00.0	38105	77	
	23:31:32.60	-26:08:56.3	16565	31	34a
	23:31:43.70	-25:58:23.8	65375	73	
	23:31:54.61	-25:53:29.2	27282	21	
2641	23:39:03.63	-24:41:18.3	30739	26	
	23:39:14.66	-24:40:11.7	8460	63	42a
	23:39:51.90	-25:14:12.8	9784	33	44a
	23:39:53.97	-24:48:06.6	31708	62	43a
	23:40:31.79	-24:30:40.1	34539	38	
	23:40:45.16	-24:41:31.4	6754	65	
	23:40:52.81	-24:53:31.1	43318	56	
	23:40:59.36	-24:31:16.3	31227	37	
	23:41:18.30	-24:31:25.4	31204	20	41e
	23:41:19.35	-25:02:08.6	15808	62	
	23:41:30.27	-25:02:32.9	15726	17	
	23:41:54.71	-24:37:54.1	17564	21	
	23:42:00.45	-25:11:21.1	9780	52	39a
	23:42:06.82	-25:03:58.2	22378	30	40e
3951	22:58:39.10	-18:47:03.9	35458	28	
	22:58:45.53	-18:42:09.0	21563	52	
	22:58:45.94	-18:26:23.0	35521	83	
	22:59:08.96	-18:32:12.2	54535	10	105a
	22:59:10.52	-18:45:42.2	21801	23	
	22:59:11.99	-18:57:58.7	45011	45	
	22:59:12.22	-18:49:57.5	21965	73	
	22:59:29.41	-18:38:41.5	32990	20	106a
	22:59:52.50	-18:17:28.4	35076	30	
	23:00:04.81	-18:55:18.0	21933	25	
	23:00:08.18	-18:44:13.4	19496	35	
	23:00:19.31	-18:34:21.4	21377	89	104a
	23:00:32.28	-18:36:59.1	42775	43	

TABLE 1—*Continued*

Cluster	α J2000	δ J2000	Velocity km s ⁻¹	Error km s ⁻¹	Emission Reference
3996	23:00:32.42	-18:47:12.7	25130	38	102a
	23:00:33.94	-18:34:56.8	56640	59	
	23:01:03.65	-18:24:17.2	9242	67	103a
	23:01:09.93	-18:51:21.5	21974	23	
	23:01:23.13	-18:47:46.3	38046	32	
	23:01:31.76	-18:27:00.2	21462	22	
	23:20:16.09	-22:00:06.5	32787	39	120e
	23:20:19.95	-21:46:14.4	25266	20	
	23:20:20.90	-21:40:20.6	42499	35	
	23:20:23.77	-21:53:38.2	39968	60	
	23:20:47.67	-22:08:57.0	7783	26	122a
	23:21:11.99	-22:15:56.0	17681	60	121a
	23:21:13.94	-21:38:34.7	33953	42	
	23:21:26.02	-21:47:58.8	36770	30	
	23:21:27.21	-21:56:52.3	24349	50	
	23:21:43.39	-22:01:32.9	34010	55	
	23:22:04.15	-22:06:57.8	33387	26	
	23:22:10.26	-21:48:53.8	37044	43	
	23:22:31.47	-21:51:03.6	7138	57	119a
	23:22:48.75	-22:13:21.1	16432	26	
23:22:49.59	-21:38:29.6	35455	32		
23:23:06.06	-21:54:36.2	33545	29		

TABLE 2
OTHER ABELL/ACO CLUSTERS OBSERVED WITHIN $10^\circ \times 45^\circ$ STRIP

Cluster	α J2000	δ J2000	Velocity km s^{-1}	Error km s^{-1}	Emission Reference	
2500	22:51:34.26	-25:38:08.3	21425	38		
	22:51:51.02	-25:33:30.9	8476	92		
	22:52:20.87	-25:15:05.6	22603	38		
	22:52:46.54	-25:41:12.6	23074	52		
	22:53:01.68	-25:32:33.1	15373	52		
	22:53:31.30	-25:33:20.7	23320	42		
	22:53:46.38	-25:29:59.0	26718	30		
	22:53:54.69	-25:16:57.6	27092	37		
	22:53:59.69	-25:27:17.0	30411	73		
	22:54:22.22	-25:31:31.5	23650	46		
	22:55:23.74	-25:37:10.7	5325	89		
	3725	20:56:06.78	-46:52:12.2	42906	28	
		20:56:41.16	-46:42:29.3	50021	65	
20:57:15.23		-46:51:14.4	61600	75		
20:57:20.67		-46:42:53.6	20480	26	59a	
20:57:32.92		-47:03:50.1	39615	67		
20:57:36.20		-46:34:06.2	24777	47	57a	
20:57:37.35		-46:39:29.2	24758	63	58a	
20:57:38.80		-46:57:05.3	49067	49		
20:57:59.19		-46:48:26.0	32270	20	60e	
20:58:28.71		-46:43:57.6	16834	30	56a	
20:58:36.81		-46:53:32.3	44883	30		
20:58:50.96		-47:01:48.0	45347	39		
20:58:55.15		-46:47:01.4	12956	35		
20:59:25.24		-46:30:37.0	13097	36	55a	
20:59:28.64		-46:41:04.3	22034	69		
20:59:30.44		-47:12:14.0	12996	22		
20:59:33.48		-46:45:06.4	13043	32	54a	
20:59:34.19		-46:57:58.4	29952	55	53a	
21:00:12.59		-46:33:10.6	44699	36		
21:00:42.76	-46:34:01.9	32096	26			
21:01:16.84	-46:41:15.4	48513	71			
3750	21:11:31.89	-49:30:22.5	28896	52		
	21:12:12.13	-49:22:33.1	16085	83		
	21:12:39.31	-49:35:00.2	26214	33		
	21:12:39.90	-49:28:49.6	50367	51		
	21:13:32.90	-49:20:42.8	28880	25		
	21:13:45.42	-49:24:05.0	49341	62		
	21:13:56.10	-49:38:02.3	49250	60		
	21:14:11.01	-49:34:31.6	49131	36	61e	
	21:14:32.00	-49:28:47.7	54349	44	64e	
	21:14:46.23	-49:32:02.7	49715	62	63a	
	21:15:16.57	-49:24:03.9	49492	53		
	21:16:06.73	-49:42:21.3	18084	77	62a	
	21:16:14.29	-49:23:17.3	16037	20		
	21:16:44.04	-49:25:54.0	18320	37		
	21:16:45.00	-49:23:26.3	21819	27		

TABLE 2—*Continued*

Cluster	α J2000	δ J2000	Velocity km s ⁻¹	Error km s ⁻¹	Emission Reference	
3757	21:16:12.82	-45:06:54.3	31429	20	70a	
	21:16:49.81	-44:54:58.9	27523	65		
	21:16:59.96	-45:11:10.3	29419	60		
	21:17:04.97	-45:18:26.0	14097	60		
	21:17:25.28	-45:34:05.6	19646	25		
	21:17:34.32	-45:00:22.8	22658	44	69a	
	21:17:42.41	-44:57:31.2	27531	42		
	21:18:12.96	-45:05:36.4	4861	11	68a	
	21:18:35.24	-45:14:31.8	29217	33		
	21:18:41.80	-45:00:25.0	9207	26		
	21:18:57.29	-45:11:23.8	22456	43		
	21:19:34.52	-45:23:04.6	2813	49	65a	
	21:19:36.56	-45:01:04.3	5298	73	67a	
	21:19:41.11	-45:07:02.6	5130	17		
	21:19:45.67	-45:20:34.1	29675	33		
	21:20:24.82	-45:21:22.5	29478	44		
	21:20:55.39	-45:08:26.2	23524	92	66a	
	3775	21:29:10.68	-43:17:12.9	47313	75	
		21:29:36.04	-43:14:53.8	5451	50	
		21:30:13.16	-42:55:07.4	19465	48	76a
		21:30:15.37	-42:59:42.6	19188	26	
21:30:25.69		-43:12:09.6	5010	69		
21:30:36.85		-43:09:04.6	4908	56	77a	
21:31:12.01		-43:11:12.6	32398	22		
21:31:19.29		-42:55:18.3	42380	47		
21:31:24.48		-43:15:33.8	5429	35	78a	
21:31:33.18		-43:18:24.8	31890	29		
21:31:36.55		-43:21:33.5	31306	60		
21:31:53.17		-43:23:52.8	26953	49		
21:32:16.56		-43:00:02.3	41855	32		
21:32:19.79		-43:17:08.0	31423	29		
21:32:21.60		-43:22:10.5	32101	75		
21:32:32.33		-43:07:34.6	42255	32		
21:32:39.56		-43:00:48.0	21943	57		
21:32:51.87		-43:25:14.0	32071	48	74a	
21:32:53.92		-43:19:53.8	31813	35		
21:33:23.02		-43:22:57.9	32455	30		
21:33:36.70		-43:28:18.6	31343	31		
21:33:50.73	-43:06:27.0	4139	96	75a		
21:34:01.70	-43:08:12.2	18532	39			
3818	21:49:00.07	-47:56:13.3	33546	48		
	21:49:01.30	-48:02:47.5	33532	38		
	21:50:04.50	-47:48:52.1	18489	26		
	21:51:01.05	-48:07:45.1	18408	29		
	21:51:34.10	-47:59:32.1	18847	27		
	21:51:37.40	-48:15:06.7	49009	63		
	21:52:05.31	-48:10:44.5	19178	18		

TABLE 2—*Continued*

Cluster	α J2000	δ J2000	Velocity km s ⁻¹	Error km s ⁻¹	Emission Reference
	21:52:19.61	-48:09:16.7	27741	65	
	21:52:49.19	-48:01:55.2	18371	28	
	21:52:58.07	-48:07:07.0	31453	29	
3821	21:50:33.46	-44:01:25.6	33536	60	
	21:51:07.08	-43:50:47.2	7861	75	
	21:51:24.80	-44:18:36.8	15293	20	
	21:51:49.81	-43:45:56.8	44330	92	
	21:52:15.49	-43:56:56.9	33502	53	
	21:52:15.55	-44:03:19.4	41893	49	
	21:52:19.73	-44:06:37.3	31438	23	
	21:53:04.85	-43:48:38.5	9941	22	
	21:53:19.21	-44:00:43.8	41874	41	
	21:53:22.55	-43:58:32.5	41826	33	
	21:53:22.59	-44:11:22.9	31438	23	
	21:53:22.85	-43:51:28.5	46495	50	
	21:54:50.08	-44:17:40.2	18568	77	
3834	22:03:25.51	-47:24:20.1	17302	55	
	22:03:31.18	-47:14:20.8	34374	43	
	22:03:55.21	-47:13:37.5	16863	44	
	22:04:13.68	-47:43:20.3	41176	86	
	22:04:27.35	-47:12:44.8	52226	86	
	22:04:28.28	-47:23:51.6	9987	36	
	22:05:22.79	-47:26:03.2	45426	39	
	22:06:09.77	-47:29:27.1	34651	24	81a
	22:06:18.22	-47:26:23.0	10018	77	82a
	22:06:19.59	-47:09:26.1	8702	39	
	22:06:29.26	-47:38:12.6	45729	51	
	22:06:50.15	-47:17:01.2	17395	21	
	22:06:58.36	-47:26:59.2	31600	23	
	22:07:11.58	-47:18:49.9	9961	96	
	22:07:22.66	-47:22:43.4	8652	34	
3839	22:07:39.63	-49:03:50.2	10761	42	
	22:08:04.19	-48:34:48.0	53409	96	
	22:08:51.99	-48:41:58.8	63523	83	
	22:09:34.64	-48:40:33.2	10184	80	
	22:10:05.75	-49:02:06.3	60487	27	84e
	22:10:25.82	-48:42:56.7	31744	65	
	22:10:43.01	-49:15:33.5	38162	89	
	22:11:13.31	-49:01:16.9	18289	89	
	22:11:18.76	-48:36:01.1	26048	63	
	22:11:38.76	-48:48:20.8	17174	36	
	22:11:46.08	-48:45:56.0	17370	39	
	22:11:53.36	-48:34:47.5	17011	80	
	22:11:56.74	-48:43:15.2	17105	27	83e
	22:12:07.21	-48:29:09.9	10290	59	
	22:12:31.64	-48:55:50.3	10964	89	
3841	22:09:15.89	-48:43:45.1	15268	30	86e

TABLE 2—*Continued*

Cluster	α J2000	δ J2000	Velocity km s ⁻¹	Error km s ⁻¹	Emission Reference
	22:09:34.56	-48:40:33.2	10570	56	
	22:09:53.22	-48:31:59.6	10531	83	
	22:09:53.50	-48:16:26.3	38118	39	
	22:09:55.35	-48:53:01.4	58347	69	
	22:10:10.07	-48:42:08.4	34029	69	
	22:10:17.81	-48:55:17.1	59658	62	
	22:10:29.75	-48:20:06.4	44441	30	
	22:10:46.98	-48:32:55.9	60157	83	
	22:10:58.87	-48:11:53.1	17372	56	
	22:11:18.76	-48:36:01.1	26079	23	
	22:11:38.76	-48:48:20.8	17331	21	
	22:11:46.08	-48:45:56.0	17452	38	
	22:11:53.36	-48:34:47.5	17079	56	
	22:11:56.74	-48:43:14.9	17170	38	85e
	22:12:07.10	-48:29:09.7	10314	60	
3842	22:13:16.43	-48:39:55.3	55416	96	
	22:10:13.61	-38:48:37.5	28633	29	
	22:11:18.50	-38:40:08.5	28578	37	
	22:11:49.85	-38:25:56.9	11078	27	
	22:11:49.92	-38:57:30.6	18340	89	
	22:11:59.51	-38:32:29.8	10999	41	
3844	22:12:18.27	-38:30:05.9	10766	31	
	22:11:30.27	-35:02:49.2	17733	32	
	22:12:15.78	-34:49:46.6	36303	47	91a
	22:12:36.03	-34:54:31.7	26888	63	90a
	22:12:58.31	-34:42:56.7	22169	23	
	22:13:02.36	-34:49:13.4	43426	35	
	22:13:08.98	-35:10:49.7	35626	45	
	22:13:17.60	-34:39:59.9	21942	24	
	22:13:33.49	-34:39:36.0	21810	26	89a
	22:13:39.48	-34:48:19.2	43639	40	
	22:13:59.81	-34:56:13.5	17518	45	87a
	22:14:21.51	-35:07:47.5	36370	65	
	22:14:30.56	-34:58:18.8	17329	25	
	22:14:43.15	-35:05:07.6	23619	80	
	22:14:43.19	-34:45:42.4	44097	48	
	22:14:43.63	-35:01:27.9	17696	29	
	22:14:46.51	-34:50:20.7	44054	44	88a
	22:15:35.20	-35:09:39.0	17845	32	2
3858	22:17:32.15	-34:24:47.4	20708	32	93e
	22:18:07.03	-34:37:26.8	24206	69	
	22:18:21.19	-34:41:10.1	44652	55	
	22:18:21.43	-34:27:54.0	49953	67	
	22:18:44.13	-34:45:34.8	46406	49	
	22:19:04.12	-34:32:58.0	20786	22	
	22:19:28.69	-34:44:24.0	45662	41	
	22:19:47.56	-34:22:28.5	23617	35	

TABLE 2—*Continued*

Cluster	α J2000	δ J2000	Velocity km s ⁻¹	Error km s ⁻¹	Emission Reference
	22:19:51.44	-34:34:51.5	46846	71	
	22:20:02.01	-35:04:58.5	46142	57	
	22:20:10.29	-34:51:16.3	46428	44	
	22:20:16.92	-34:40:04.9	12332	24	
	22:20:19.16	-34:55:13.5	20499	37	
	22:20:32.52	-35:09:48.2	46405	89	
	22:21:02.89	-34:59:08.0	9243	31	
	22:21:04.04	-34:35:49.4	49640	31	92e
3861	22:18:06.93	-37:28:50.1	40911	69	
	22:18:06.97	-36:52:16.0	42655	33	
	22:18:07.22	-36:56:09.1	42509	53	
	22:18:31.09	-37:36:05.2	41894	55	
	22:18:47.87	-37:10:58.2	45702	48	
	22:19:44.92	-37:06:40.5	10203	24	94e
	22:20:37.06	-37:19:01.7	22056	20	
	22:20:42.58	-37:31:38.4	28164	45	
	22:21:00.94	-37:17:10.8	21910	77	
	22:21:03.47	-37:30:50.8	42601	75	
	22:21:28.39	-37:07:51.6	14523	65	
	22:22:06.70	-37:19:38.8	50111	77	
3892	22:35:49.19	-30:54:38.2	8319	55	
	22:36:01.97	-30:38:18.5	63269	71	
	22:37:10.09	-30:44:42.4	8357	80	95a
	22:37:19.40	-30:40:58.4	35455	52	
	22:37:22.43	-30:44:44.6	8357	73	
	22:37:51.36	-30:40:10.7	35002	29	
	22:37:51.90	-30:37:03.5	33485	57	
	22:38:35.09	-30:54:55.4	14792	26	
3896	22:37:18.90	-38:02:46.1	18082	80	
	22:37:21.46	-37:37:11.6	16749	38	96e
	22:37:41.20	-37:34:07.5	17645	55	
	22:37:49.57	-37:44:13.4	22670	51	
	22:37:54.28	-38:06:50.7	17428	73	
	22:38:03.32	-37:49:36.1	46053	75	
	22:38:06.40	-38:14:34.0	34229	41	
	22:38:07.08	-38:01:26.8	21806	29	
	22:38:51.99	-37:50:18.7	45743	44	
	22:39:02.35	-37:45:27.3	46314	83	
	22:39:09.79	-38:09:22.2	34682	41	
	22:39:28.49	-38:06:52.6	34605	62	
	22:39:31.44	-37:31:41.0	13575	83	
	22:39:39.39	-37:51:27.0	46321	60	
	22:39:40.71	-37:43:44.3	21663	25	
	22:39:52.01	-37:44:44.5	21816	42	
	22:39:53.32	-37:56:32.6	22030	57	
	22:40:19.98	-37:49:47.0	19235	89	
	22:40:25.11	-37:41:23.8	22472	96	

TABLE 2—*Continued*

Cluster	α J2000	δ J2000	Velocity km s ⁻¹	Error km s ⁻¹	Emission Reference
3920	22:40:51.68	-38:03:54.2	21965	80	97a
	22:41:04.32	-37:45:50.3	23675	89	
	22:47:04.18	-40:49:02.4	40905	36	
	22:47:23.74	-40:52:55.9	20015	16	
	22:47:41.37	-40:56:54.7	20275	86	
	22:47:42.07	-40:59:22.6	19965	24	
	22:48:06.29	-41:00:10.9	20215	26	
	22:48:15.69	-40:49:56.6	24144	56	
	22:49:10.01	-41:00:58.5	37976	27	
	22:49:28.65	-40:53:33.6	37815	41	
	22:49:32.29	-41:03:41.6	37911	33	
	22:49:40.17	-40:28:33.4	38266	40	
	22:49:46.79	-40:56:01.3	37141	29	
	22:49:57.21	-40:35:06.8	39352	31	
22:50:23.53	-40:50:44.2	40201	44		
22:51:01.06	-40:40:42.5	40689	62		
22:51:05.67	-41:05:48.3	26021	48		
3928	22:50:27.58	-33:36:05.3	26944	32	
	22:51:38.06	-33:57:07.6	9163	46	
	22:51:38.46	-33:31:21.9	35272	75	
	22:51:46.18	-33:25:22.6	33187	75	
	22:51:58.82	-33:11:37.5	35144	25	
	22:52:13.26	-33:58:51.0	29343	34	
	22:52:18.49	-33:19:51.7	30755	26	
	22:52:42.15	-33:40:38.9	22994	60	
	22:52:59.45	-33:14:03.3	25176	53	
	22:53:26.81	-33:27:45.6	35819	80	
	22:53:56.19	-33:22:30.8	35645	38	
	22:54:01.53	-33:44:07.0	8760	73	
	22:54:17.76	-33:49:56.2	8221	71	
	22:54:14.46	-40:08:55.0	9427	53	
3944	22:54:20.54	-40:16:35.0	31073	31	98a 100a
	22:54:31.11	-40:17:57.0	13365	62	
	22:54:44.82	-39:55:58.3	18212	73	
	22:55:00.68	-39:53:05.0	13152	26	
	22:55:30.31	-40:07:31.5	30939	51	
	22:56:01.87	-39:50:13.3	53417	49	
	22:56:39.15	-40:16:47.6	18415	52	
	22:56:39.78	-40:00:38.7	31083	53	
	22:56:45.65	-39:47:11.5	18206	65	
	22:56:55.66	-40:07:14.6	38239	47	
	22:57:32.78	-39:50:14.8	27126	24	
	22:57:37.83	-39:56:00.5	22793	69	
	22:57:54.12	-40:02:22.6	27270	26	
	22:58:21.02	-40:17:11.6	9656	29	
3959	22:58:23.92	-40:07:45.1	10218	69	99a
	23:00:39.61	-33:27:35.3	8738	24	

TABLE 2—*Continued*

Cluster	α J2000	δ J2000	Velocity km s ⁻¹	Error km s ⁻¹	Emission Reference
	23:00:50.04	-33:36:32.7	26054	42	
	23:01:05.81	-33:09:04.5	16403	86	108a
	23:01:22.90	-33:38:39.3	26268	83	
	23:01:39.88	-33:11:26.7	16419	21	107e
	23:01:48.26	-33:43:37.1	53091	89	110a
	23:02:03.12	-33:26:51.0	26148	77	
	23:02:09.48	-33:05:51.8	10583	35	
	23:02:22.35	-33:32:25.2	25177	65	112e
	23:02:26.46	-33:48:57.5	32432	27	
	23:02:28.77	-33:23:02.4	26152	26	109e
	23:02:40.27	-33:11:57.6	26202	22	
	23:02:41.21	-33:31:15.9	4915	80	
	23:02:51.87	-33:23:22.5	19761	31	
	23:03:08.98	-33:48:06.1	17759	92	111a
	23:03:21.01	-33:36:17.0	25892	25	
	23:03:42.17	-33:11:48.8	16168	29	
	23:03:47.50	-33:38:43.3	26578	22	
	23:04:22.69	-33:21:53.7	41728	27	
	23:04:22.78	-33:10:21.0	16452	35	
	23:04:42.22	-33:17:27.7	18110	67	
	23:04:42.44	-33:44:24.9	25250	28	
3978	23:09:26.48	-28:48:11.1	14959	36	
	23:09:34.44	-28:34:54.3	14734	96	115a
	23:09:42.35	-28:57:26.7	26108	20	
	23:09:44.55	-29:13:35.5	31197	35	
	23:09:53.59	-29:05:15.9	14975	13	118a
	23:10:27.73	-28:41:00.7	26028	38	
	23:10:36.06	-28:38:55.8	26157	29	
	23:10:46.46	-28:38:59.3	26207	23	
	23:10:58.60	-29:01:09.2	34407	27	116a
	23:11:00.79	-28:56:38.2	32050	41	
	23:11:21.26	-28:41:13.2	26194	25	
	23:11:21.91	-28:51:29.7	26535	29	
	23:11:34.87	-28:41:15.7	41323	39	
	23:11:36.24	-28:59:52.7	31461	27	
	23:11:39.17	-29:06:38.2	34949	28	117a
	23:11:46.82	-28:31:45.0	1393	62	
	23:12:09.60	-28:25:54.3	9766	18	
	23:12:22.66	-29:04:51.7	14875	46	113a
	23:12:23.82	-28:43:44.8	26038	28	
	23:12:26.95	-29:02:07.7	61201	59	
	23:12:56.72	-28:50:45.6	35091	22	
	23:13:06.76	-28:58:56.9	9713	50	114a

TABLE 3
ABELL/ACO GALAXIES IN GRUS-INDUS SAMPLE

Cluster	α J2000	δ J2000	Velocity km s ⁻¹	Error km s ⁻¹	Emission Reference
3148	3:36:44.20	-32:53:35.0	19811	67	
	3:37:12.80	-32:28:35.2	31423	24	
	3:37:17.17	-32:51:41.6	35416	43	
	3:37:32.06	-32:26:01.6	31753	25	
	3:37:33.33	-32:21:15.6	11799	55	
	3:38:05.93	-32:25:33.3	35503	23	
	3:38:13.96	-32:51:41.8	32237	22	
	3:38:17.97	-33:07:15.4	32551	21	
	3:38:44.30	-32:39:18.8	39024	41	
	3:38:45.11	-32:30:30.8	35280	25	
	3:38:45.15	-32:47:58.0	32091	24	
	3:38:48.07	-32:42:07.7	39332	31	
	3:39:11.01	-32:33:52.0	13393	36	46e
	3:39:11.53	-33:03:14.8	32615	31	
	3:39:17.68	-32:51:26.6	28329	23	
	3:39:25.05	-32:21:26.3	38898	40	
	3:39:31.37	-32:45:58.8	37584	36	
	3:39:38.04	-32:37:09.5	38299	33	
	3:39:39.27	-32:49:37.8	28318	46	
	3:39:55.73	-32:24:50.2	13347	73	45a
3:40:03.72	-32:56:57.8	17910	22		
3:40:24.83	-32:34:48.4	28549	21		
3:40:45.90	-32:30:36.9	28139	21		
3166	3:45:02.73	-32:43:05.2	22184	44	
	3:45:37.17	-32:30:02.6	32289	30	
	3:46:11.16	-32:23:24.6	32722	62	
	3:46:31.29	-33:01:49.9	31796	83	
	3:46:40.60	-32:53:09.2	27558	47	
	3:46:42.82	-32:41:08.9	30501	26	
	3:46:43.83	-32:48:45.6	35126	33	
	3:46:59.31	-32:40:10.6	34956	39	
	3:47:09.19	-32:49:22.1	27156	57	
	3:47:21.31	-32:21:12.0	32379	38	
	3:47:33.93	-32:51:35.9	34862	51	
	3:47:46.63	-32:35:54.8	39229	47	
	3:47:47.84	-32:56:16.6	27338	45	
	3:47:57.11	-32:28:12.2	18023	89	
	3:48:01.11	-33:04:09.1	18138	86	
	3:48:38.62	-32:57:34.7	33406	41	
3:48:57.16	-32:37:17.1	21876	21		
3169	3:47:06.34	-33:25:33.7	16624	30	48e
	3:47:26.29	-33:20:02.4	49385	65	
	3:47:34.15	-33:06:50.9	49970	53	
	3:47:49.51	-33:18:50.5	49615	92	
	3:47:53.23	-33:08:02.0	33651	25	
	3:48:01.11	-33:04:09.1	18208	21	
	3:48:08.82	-33:25:25.0	48578	51	

TABLE 3—*Continued*

Cluster	α J2000	δ J2000	Velocity km s ⁻¹	Error km s ⁻¹	Emission Reference
	3:48:23.46	-33:37:04.5	20222	34	
	3:48:28.98	-33:19:44.2	35259	22	
	3:48:32.08	-33:27:18.8	50271	52	
	3:48:38.07	-33:23:06.3	34783	24	
	3:48:39.39	-33:44:14.2	16295	34	
	3:48:47.98	-33:14:09.6	68901	89	
	3:48:48.19	-33:02:30.7	35281	32	
	3:49:11.76	-33:36:55.8	61313	71	
	3:49:13.45	-33:28:20.2	50097	47	
	3:49:20.91	-33:46:29.5	35196	46	
	3:49:30.00	-33:36:26.1	49048	46	
	3:49:50.17	-33:35:28.9	49108	53	
	3:50:20.21	-33:19:22.8	22747	89	47a
3171	3:47:37.97	-34:21:28.1	16149	19	
	3:48:05.19	-34:16:29.0	38541	62	
	3:48:06.15	-33:49:58.1	33072	43	
	3:48:17.04	-34:03:00.6	37659	55	
	3:48:27.47	-34:21:32.4	16139	23	
	3:48:31.43	-34:05:54.9	48731	46	
	3:48:39.28	-34:02:48.6	49316	50	
	3:48:39.39	-33:44:13.9	16218	38	
	3:48:48.09	-34:00:20.1	49592	69	
	3:49:07.77	-33:48:16.2	37502	32	
	3:49:09.90	-33:53:07.7	33828	33	
	3:49:12.58	-34:21:24.5	20137	80	
	3:49:16.77	-34:11:02.5	37641	52	
	3:49:20.91	-33:46:29.5	35280	28	
	3:49:30.35	-34:09:06.6	35447	48	
	3:49:37.33	-33:48:00.9	43645	40	
	3:49:50.17	-33:35:28.9	49075	65	
	3:50:22.21	-33:56:53.6	7041	35	49e
	3:50:25.81	-33:47:09.5	41506	41	
	3:50:26.44	-34:11:52.6	33593	45	
3197	3:57:46.59	-30:30:13.3	49762	62	
	3:58:24.14	-30:17:38.6	29917	24	
	3:58:38.51	-30:20:09.5	43482	45	
	3:58:48.14	-30:08:04.2	28353	29	
	3:58:48.29	-30:16:35.3	30314	21	
	3:58:53.69	-30:14:05.4	28982	26	
	3:59:08.86	-30:18:09.6	28272	77	51a
	3:59:10.74	-30:10:12.4	27790	23	
	3:59:13.79	-30:30:43.4	28734	63	
	3:59:17.81	-30:01:29.0	29687	39	
	3:59:38.18	-29:59:56.0	29384	24	
	3:59:43.44	-30:27:04.9	50231	50	
	3:59:47.78	-30:04:05.9	30251	57	50a
	4:00:24.42	-30:20:31.7	28538	39	

TABLE 3—*Continued*

Cluster	α J2000	δ J2000	Velocity km s ⁻¹	Error km s ⁻¹	Emission Reference
	4:00:24.91	-29:57:47.9	29364	25	
	4:00:30.31	-30:06:56.5	28992	26	
	4:00:35.20	-30:39:42.7	42909	47	
	4:01:00.32	-30:36:33.2	28881	34	
	4:01:17.03	-30:14:29.5	29124	27	
	4:01:35.26	-30:18:18.5	29268	37	
	4:01:39.58	-30:29:27.6	30372	41	
3200	3:59:37.47	-31:17:22.2	59328	89	
	3:59:43.21	-30:51:30.3	53133	80	
	3:59:59.94	-30:57:53.5	42724	39	
	4:00:20.43	-31:03:11.9	28798	69	
	4:00:34.17	-31:12:12.6	49796	52	
	4:00:34.35	-31:24:37.8	60978	60	
	4:00:41.59	-30:49:50.0	1531	71	
	4:00:44.94	-31:09:46.5	52237	53	
	4:01:04.36	-31:30:08.9	18125	17	
	4:01:18.71	-31:02:57.9	21241	96	52a
	4:01:33.51	-31:05:33.6	14905	75	
	4:01:34.32	-31:01:11.3	15036	60	
	4:01:36.01	-31:29:39.3	19723	18	
	4:01:49.43	-31:29:09.9	19932	29	
	4:02:21.31	-31:13:23.3	28844	21	
	4:02:22.66	-30:56:39.7	43178	44	
	4:02:52.25	-31:24:55.3	40995	33	
	4:02:55.24	-31:20:18.9	17885	20	
3205	4:00:52.97	-27:08:39.4	23095	96	
	4:01:19.22	-26:52:57.0	19057	34	
	4:01:52.90	-26:39:47.8	21624	47	
	4:02:21.90	-26:56:50.3	19141	89	
	4:02:25.99	-26:52:25.5	22237	92	
	4:02:27.54	-26:48:30.2	56910	56	
	4:02:52.33	-26:53:13.3	56790	62	
	4:03:34.61	-26:33:46.9	38338	65	
	4:03:35.53	-26:57:29.7	25917	39	
	4:03:52.98	-26:44:55.1	32869	65	
	4:03:59.66	-26:55:41.7	25923	47	

TABLE 4
EMISSION LINE GALAXY VELOCITIES

Cluster	Galaxy Reference	Velocity (km s ⁻¹)	Error (km s ⁻¹)	Lines Found
A2557	1a	28074	45	OII ^{S/N}
	2a	19648	30	OII, H β
A2585	3a	26793	20	OII, (H β , OIII)
	4a	13613	30	OII
	5a	8386	30	OII
	6a	21308	20	OII, (H β)
	7e	56905	20	OII, H β , OIII ₅₀₀₇ , (OIII ₄₉₅₈)
A2599	8a	26839	44	OII
	9a	26651	20	OIII ₄₉₅₈ , (H β), OIII ₅₀₀₇)
	10e	1709	20	H β , OIII, (H γ)
	11e	33158	20	OII, H β , OIII ₄₉₅₈ , (OIII ₅₀₀₇)
	12a	25938	20	OII, (H β)
	13a	27213	41	OII ^{S/N}
	14a	34098	20	OII, H β , OIII
A2600	15a	18649	33	OII ^{S/N}
	16a	26094	37	OII
	17a	18118	20	OII, H β , OIII
	18a	18127	20	OII, H β
	19a	18075	40	OII
	20a	18644	30	OII
	21a	16389	26	OII, OIII
	22a	35358	30	OII
	23a	35575	30	OII
	24a	34289	37	OII ^{S/N}
	25a	34522	20	OII, OIII ₄₉₅₈ , (OIII ₅₀₀₇)
	26e	36890	30	OII, (H β)
	27a	36717	31	OII
A2601	28e	37842	20	OII, H β , OIII
	29e	2765	20	H β , OIII (NeIII, H ϵ , H δ , H γ , OIII 4363, HeI)
	30a	20201	34	OII, H β
A2608	31a	35472	37	OII
	32a	19579	20	OII, H β
	33a	14110	20	OII, H β
A2609	34a	16504	20	OII, OIII, (H β)
	35a	27208	52	OII
	36e	63277	20	OII, H β , OIII ₅₀₀₇ , (OIII ₄₉₅₈)
	37a	32976	20	OII, H β
	38e	25548	30	OII, H β , OIII
A2641	39a	9788	20	OII, H β , OIII ₄₉₅₈ , (OIII ₅₀₀₇)
	40e	22378	30	OII, OIII ₅₀₀₇ , (OIII ₄₉₅₈)
	41e	31204	20	OII, H β , OIII
	42a	8414	20	H β , OIII ₅₀₀₇ , (OII, OIII ₄₉₅₈)
	43a	31675	37	OII
	44a	9896	20	OII, OIII ₅₀₀₇ , (OIII ₄₉₅₉)
A3148	45a	13318	23	H β , OIII
	46e	13393	36	H β , OIII

TABLE 4—*Continued*

Cluster	Galaxy Reference	Velocity (km s ⁻¹)	Error (km s ⁻¹)	Lines Found	
A3169	47a	22438	34	OII, H β	
	48e	16624	30	OII, H β , OIII	
A3171	49e	7041	35	H β , OIII	
A3197	50a	30391	26	OII, OIII	
	51a	28106	24	OII, H β , OIII	
A3200	52a	21276	23	OII, H β , OIII	
A3725	53a	29832	30	OII, (H β)	
	54a	12960	20	OII, H β , OIII	
	55a	12978	20	OII, H β , OIII	
	56a	16897	37	OII	
	57a	24764	30	OII	
	58a	24914	20	OII, H β , OIII, (H γ)	
	59a	20621	31	OII	
	60e	32270	20	OII, OIII	
	A3750	61e	49131	36	OII
		62a	18288	20	OII, H β , OIII
63a		49610	37	OII	
A3757	64e	54349	44	OII	
	65a	2766	20	H β , OIII, (H γ , HeI)	
	66a	23532	22	OII, H β , OIII	
	67a	5135	20	H β , OIII	
	68a	4861	20	H β , OIII, (NeIII ₃₈₆₉ , HeI)	
	69a	22678	35	OII, OIII	
A3775	70a	31429	20	OII, H β , OIII	
	74a	31944	44	OII	
	75a	4283	20	NeIII, H ϵ , H δ , H γ , H β , OIII, HeI	
	76a	19585	20	OII, H β , OIII ₅₀₀₇ , (OIII ₄₉₅₈)	
	77a	4930	20	H β , OIII ₅₀₀₇ , (OIII ₄₉₅₈)	
A3834	78a	5419	20	H β , OIII ₅₀₀₇ , (OIII ₄₉₅₉)	
	81a	10281	26	H β , OIII	
	82a	8645	33	OIII	
A3839	83e	17105	27	OII, H β , OIII	
	84e	60487	27	OII, OIII	
A3841	85e	17170	38	OII, OIII	
	86e	15268	30	OII, H β , OIII	
A3844	87a	17530	30	OII ^{S/N}	
	88a	43925	34	OII ^{S/N}	
	89a	21965	30	OII ^{S/N}	
	90a	26690	34	OII ^{S/N}	
	91a	36303	50	OII ^{S/N}	
A3858	92e	49640	31	OII, H β , OIII	
	93e	20708	32	OII, H β , OIII	
A3861	94e	10203	24	H β , OIII	
A3892	95a	8437	24	H β , OIII	
A3896	96e	16749	38	OII, H β , OIII	
	97a	22061	24	OII, H β , OIII	
A3928	98a	8204	23	H β , OIII	

TABLE 4—*Continued*

Cluster	Galaxy Reference	Velocity (km s ⁻¹)	Error (km s ⁻¹)	Lines Found
A3944	99a	10169	33	H β , OIII
	100a	9468	22	H β , OIII
	101a	30786	23	OII, OIII
A3951	102a	25295	20	OII, OIII
	103a	9233	29	OII, H β , OIII
	104a	21524	20	OII, H β , OIII
	105a	54535	20	OII, H β , OIII
	106a	32990	26	OII, H β
A3959	107e	16419	21	OII, OIII ₅₀₀₇ , (H β , OIII ₄₉₅₈)
	108a	16480	20	OII, H β , OIII ₅₀₀₇ , (OIII ₄₉₅₈)
	109e	26152	26	OII, H β , OIII
	110a	53016	38	OII, (H β)
	111a	17735	20	OII, H β , OIII
A3978	112e	25177	65	OII
	113a	14864	20	OII, H β , OIII
	114a	9738	20	OII, H β , OIII ₅₀₀₇ , (OIII ₄₉₅₈)
	115a	14952	20	OII, H β , OIII
	116a	34346	22	OII, OIII ₄₉₅₈ , (OIII ₅₀₀₇)
	117a	34924	24	OII
	118a	14975	21	OII, OIII ₅₀₀₇ , (OIII ₄₉₅₈)
	119a	7127	26	H β
A3996	120e	32787	39	OII, OIII ₄₉₅₈ , (H β , OIII ₅₀₀₇)
	121a	17632	21	OII ^{S/N} , OIII ^{S/N} , (H β) ^{S/N}
	122a	7743	20	OIII, (OII)

^{S/N}Low signal to noise

Galaxy references with an (a) or an (e) indicate which velocity, (a) absorption or (e) emission, is published in Table 1.

Emission lines denoted within parentheses indicate that the line was detected but not included in the velocity determination.

TABLE 5A
CLUSTERS WITHIN AQUARIUS CANDIDATE REGION OBSERVED IN THIS PROGRAM

Cluster	μ km s ⁻¹	C_{BI} km s ⁻¹	σ km s ⁻¹	S_{BI} km s ⁻¹	N
A2523	38016	38037	776	818	4
A2547	44672		360		3
A2548 ^a	32771	33168	799	81	4
A2553	34279	34272	763	189	7
A2555	33114		322		3
A2556	26257	26247	154	164	4
A2557	51653	51631	1327	1397	6
A2579	33660	33363	882	735	6
A2585	56624	57113	1314	981	5
A2599	26634	26666	399	407	8
A2600	36049	36110	1452	1520	12
A2600 ^{b/f}	18283	18286	395	403	7
A2601	33357	33624	819	587	7
A2608	14927	14907	742	805	5
A2609	40449	41148	1763	2049	6
A2609 ^{b/f}	32944	32932	124	134	4
A2641	N/A				
A3951	21446	21728	822	298	7
A3996	34619	34423	1606	1743	8

TABLE 5B
CLUSTERS WITHIN AQUARIUS CANDIDATE REGION OBSERVED BY OTHERS

Cluster	μ km s ⁻¹	N	Reference
A2509	69180	1	Ciardullo
A2521	40200	2	Struble & Rood
A2528	28650	1	Ciardullo
A2531	52230	1	Ciardullo
A2534	59280	3	Struble & Rood
A2536	59130	1	Ciardullo
A2538	24850	45	Zabludoff
A2539	52050	1	Ciardullo
A2541	30540	1	Ciardullo
A2546	33570	1	Ciardullo
A2550	46290	1	Struble & Rood
A2554	33240	28	Zabludoff
A2565	38130	1	Ciardullo
A2566	24630	1	Ciardullo

TABLE 5C
CLUSTERS OUTSIDE AQUARIUS CANDIDATE BUT WITHIN OBSERVED STRIP

Cluster	μ km s ⁻¹	C_{BI} km s ⁻¹	σ km s ⁻¹	S_{BI} km s ⁻¹	N
A2500	23009	23132	909	915	6
A3725	N/C				
A3750	49483	49442	449	425	6
A3757	28807	29447	1002	993	6
A3775	31867	31868	435	447	9
A3817	63620	63461	557	520	5
A3818	18647	18524	358	397	5
A3821	43283	41864	2089	41	5
A3834	45555	45636	283	299	5
A3839	17461	17184	571	431	4
A3841	17281	17284	153	160	5
A3842	N/A				
A3844	17624	17633	203	211	5
A3844 ^{b/f}	22385	21972	836	203	4
A3844 ^{b/f}	43804	43810	326	349	4
A3861	N/A				
A3858	46929	46281	1659	1347	10
A3892	34647		1458		3
A3896	46108	46144	723	560	7
A3896 ^{b/f}	21939	22036	1119	491	10
A3920	38917	38875	1397	1477	9
A3928	33595	35172	2603	1780	7
A3944	N/C				
A3959	26056	26165	413	300	7
A3959 ^{b/f}	16885	16365	826	152	6
A3978	26181	26124	171	99	7

TABLE 5D
CLUSTER VELOCITIES WITHIN GRUS-INDUS

Cluster	μ km s ⁻¹	C_{BI} km s ⁻¹	σ km s ⁻¹	S_{BI} km s ⁻¹	N
A3148	30600	30834	1983	2352	10
A3166	33115	33121	1601	1740	9
A3169	49509	49517	586	612	8
A3171	35311	35278	2142	2207	9
A3197	29190	29185	748	775	17
A3200	51720				3
A3205	56850				2

^a $R = 0$ cluster, according to ACO criteria

^{b/f}Possible foreground/background contamination.

Discovery of Extreme Examples of Superclustering in Aquarius

D. Batuski¹, C. Miller, and K. Slinglend¹

Department of Physics and Astronomy, University of Maine, Orono, ME 04469-5709

C. Balkowski¹, S. Maurogordato, V. Cayatte¹, and P. Felenbok

Observatoire de Paris, DAEC, Unité associée au CNRS, D0173, et à l'Université Paris 7,
92195 Meudon Cedex, France

and

R. Olowin

Department of Physics and Astronomy, St. Mary's College, Moraga, CA 94575

Received _____; accepted _____

¹Visiting Astronomer, European Southern Observatory, La Silla, Chile.

ABSTRACT

The results of spectroscopic observations of 46 $R \geq 1$ clusters of galaxies from the Abell (1958) and Abell, Corwin, & Olowin (1989 - hereafter ACO) catalogs are presented. The observations were conducted at the ESO 3.6m telescope with the MEFOS multiple-fiber spectrograph. Thirty-nine of the clusters lie in a $10^\circ \times 45^\circ$ strip of sky that contains two supercluster candidates (in Aquarius and Eridanus). These candidates were identified by a percolation analysis of the Abell and ACO catalogs, using estimated redshifts for clusters that had not yet been measured. With our measurements and redshifts from the literature, the target strip is now 87% complete in redshift measurements for $R \geq 1$ ACO clusters with $m_{10} \leq 18.3$. Seven other clusters were observed in a supercluster candidate in the Grus-Indus region. Seven hundred and thirty-seven galaxy redshifts were obtained in these 46 cluster fields.

We find that one of the supercluster candidates is a collection of 14 $R \geq 1$ ACO/Abell clusters with a spatial number density that is $20\times$ the average spatial density for rich ACO clusters. This overdensity has a maximum extent of $\sim 110h^{-1}$ Mpc, making it the longest supercluster composed only of $R \geq 1$ clusters to be identified to date. This filament of clusters runs within 7° of the line of sight in the Aquarius region, and on its high- z end, four $R = 0$ ACO clusters (three of which are $R = 1$ in the Abell catalog) appear to bridge gaps to other clusters, extending the structure to $\sim 150h^{-1}$ Mpc. Our analysis also reveals that another supercluster, consisting of nine rich clusters with an extent of $\sim 75h^{-1}$ Mpc, runs roughly perpendicular to Aquarius near its low-redshift end. Both of these superclusters are quite filamentary. Fitting ellipsoids to each set of clusters, we find axis ratios (long-to-midlength axis) of 4.3 for Aquarius and 3.0 for Aquarius-Cetus. Two such filaments in a relatively

limited volume might be surprising, unless rich clusters generally can be found in elongated aggregations. We fit ellipsoids to all $N \geq 5$ clumps of clusters (at $b = 25h^{-1}$ Mpc) in the measured- z Abell/ACO $R \geq 1$ clusters sample. The frequency of filaments with axis ratios ≥ 3.0 ($\sim 20\%$) was nearly identical with that found among ‘superclusters’ in Monte Carlo simulations of random and random-clumped cluster samples, however, so the rich Abell/ACO clusters have no particular tendency toward filamentation.

The Aquarius filament also contains a ‘knot’ of six $R \geq 1$ clusters at $z \sim 0.11$, with five of the clusters close enough together to represent an apparent overdensity of $150 \bar{n}$. There are three other $R \geq 1$ cluster density enhancements similar to this knot at lower redshifts: Corona Borealis, the Shapley Concentration, and another grouping of seven clusters in Microscopium. All four of these dense superclusters appear near the point of breaking away from the Hubble Flow, and some may now be in collapse, but there is little indication of any being virialized. With four such objects, studies of them as a class may now lead to much greater insight into large-scale processes.

Subject headings: galaxies: redshifts, clusters — large-scale structure — superclusters

1. Introduction

In the last two decades, several important discoveries of large-scale structure have been made through magnitude-limited redshift surveys of individual galaxies. The first was the Coma/A1367 supercluster and void combination (Gregory & Thompson 1978, Tift & Gregory 1988), which turned out to be part of the ‘Great Wall’ and ‘bubble’ structures of the de Lapparent et al. (1988 and 1991) CfA redshift survey ‘slices.’ Later came Perseus-Pisces (Gregory, Thompson & Tift 1981), the Hercules supercluster (Tarenghi et al. 1979, Chincarini, Rood and Thompson 1981, Gregory and Thompson 1984), the Local Supercluster (Yahil et al. 1980, Tully 1982, and the early Center for Astrophysics survey work – Huchra et al. 1983), the Bootes void (Kirshner, et al. 1981), and the Hydra-Centaurus supercluster (Chincarini & Rood 1979), most recently thoroughly mapped along with the slightly more distant region of the ‘Great Attractor’ by Dressler (1988 and 1991). All of these efforts to map using magnitude-limited surveys of individual galaxies (and a few other, not complete samplings of some apparent supercluster regions) have identified structures of order $30 - 100 h^{-1}$ Mpc or more, but they are limited to volumes only about $100 h^{-1}$ Mpc deep. (Throughout this paper $h = H_0/100 \text{ km s}^{-1} \text{ Mpc}^{-1}$.) The Sloan Digital Sky Survey and the 2dF Survey being undertaken in Australia will, with a few years work, provide redshifts for the $\sim 10^6$ galaxies needed to map scales of a few hundred megaparsecs with such tracers. To study such scales now, one needs to sample more sparsely, perhaps by using pencil-beam surveys to probe deeply with individual galaxies (*e. g.*, Postman, Huchra and Geller 1986, Kirshner et al. 1987, Broadhurst *et al.* 1990, Small et al. 1998) or by randomly sampling galaxies in strips across larger areas of the sky as in the Las Campanas survey (Shectman et al. 1996)

Rich galaxy clusters are potentially excellent tracers of mass on the larger scales. With an average spatial separation of $\sim 50h^{-1}$ Mpc they are efficient for mapping scales

approaching those measured by the COBE satellite. Recent analyses of clusters from the Abell (1958) and Abell, Corwin, Olowin (1989, hereafter ACO) catalogs reveal evidence of three-dimensional superclustering on scales of 50-100 h^{-1} Mpc (*e.g.*, Miller et al. 1998, Batuski & Burns 1985b, Batuski et al. 1991, Postman, Geller & Huchra 1986, Postman, Huchra, & Geller 1992, Bahcall & Soniera 1983, Tully 1987, and Tully et al. 1992). We also note that rich (Abell/ACO) clusters are primary constituents of all the superclusters mentioned in the preceding paragraph.

However, less than one third of the Abell/ACO clusters have measured redshifts (and most of these have only one or two galaxies measured (Struble & Rood 1991b, Postman et al. 1992), although recent multi-fiber spectrographic cluster surveys such as Katgert et al. (1996) and Slingsend et al. (1998) have started to improve this situation). Single-galaxy measurements lead to substantial uncertainties in the cluster redshifts because of the possibility of measuring a foreground or background galaxy not associated with the given cluster (such projection effects being important in about 14% of Abell cluster fields with only a single previously published redshift measurement, according to Miller et al. 1998), or the possibility of measuring an ‘outlier’ in a cluster’s velocity distribution, which can introduce an error of 500 km s⁻¹ or more about 36% of the time (Miller et al. 1998). The projection problem is especially dangerous for part of the region targeted for this redshift survey, because of the very high surface number density of rich clusters. Our effort here has been an attempt to minimize these projection effects by collecting 20 or more redshifts per cluster field and then to use the resulting high-confidence redshift data to investigate superclusters of Abell/ACO clusters.

We have used MEFOS (Meudon-ESO Fiber Optic Spectrograph, see Felenbok et al. (1997) for a description) on the 3.6-m telescope at ESO to observe clusters in a 10° × 45° strip of sky that includes two particularly interesting supercluster candidates (SCCs), one in

Aquarius and one in Eridanus, to determine the significance of the apparent superclustering. Another nearby (Grus-Indus) supercluster candidate was also observed. Our sample was limited to ACO richness class $R \geq 1$ clusters, with one or zero measured redshifts in the literature, at high galactic latitude ($|b| > 30^\circ$).

Our first run of this program took place in August 1994 and the second was in September 1995. Two clusters were also observed in May 1995. We observed 39 clusters in the Aquarius-Eridanus strip (targeting to get 20 or more redshifts per cluster field) and seven clusters in the Grus-Indus SCC. We have, to this point, completed 87% of the redshift survey of the strip to $m_{10} \leq 18.3$ (estimated $z < 0.16$). We had 47 target clusters in the strip to this magnitude limit, eight of which had redshifts in the literature, and we obtained redshifts of 33 more. Six remain with unmeasured redshifts, including three that we observed but for which we obtained insufficient data for a cluster velocity determination. A preliminary report on this survey was given in Slingsend et al. (1995), and the final results are presented here.

Section 2 defines the sample of clusters observed in our primary target strip, and Section 3 summarizes the procedures for conducting the observations and reducing the data. The cluster redshift results are presented in Section 4 for both the Aquarius-Eridanus strip and Grus-Indus, along with a discussion of our analyses of the Aquarius superclusters. Section 5 contains our conclusions.

2. Cluster Sample in the Aquarius-Eridanus Strip

Our entire sample is made up of $R \geq 1$ ACO clusters within a $10^\circ \times 45^\circ$ strip of sky in the southern hemisphere (see Fig. 1). Each point in Fig. 1 represents an $R \geq 1$ cluster with $m_{10} \leq 18.3$. We used the ACO richness classification for consistency throughout the strip,

and we note that clusters on the northern end of the strip (north of $\delta = -27^\circ$) were also in Abell’s (1958) original catalog, classified in richness with a variable background subtraction in the member galaxy count, rather than the global background subtraction of ACO. The ACO m_{10} magnitude estimations were also used throughout our study.

This particular strip was chosen so as to include two apparent overdensities in the spatial distribution of rich clusters. These overdensities (SCCs) were identified using a percolation algorithm based upon the redshifts from the literature or redshifts estimated from the magnitude of the tenth brightest cluster member, using the $m_{10} - z$ relation of ACO. Distances were calculated using (Sandage 1975)

$$D = \frac{cz}{H_o} \frac{(1 + \frac{z}{2})}{(1 + z)} \quad (1)$$

for a Friedman universe with $q_0 = 0$. The percolation parameter used to identify these apparent superclusters was $30 h^{-1}$ Mpc, which corresponds to a spatial cluster density of about five times the average ACO cluster spatial number density of $8 \times 10^{-6} h^3 \text{ Mpc}^{-3}$ (Miller et al. 1998). Since most of the clusters had only estimated redshifts, these two tentative supercluster identifications were considered simply as promising targets in the selection of the strip for observing. The clusters in this strip are at high galactic latitude ($b \sim -50^\circ$ to -70°), so that obscuration is not a concern.

There has been some discussion in the literature concerning the adequacy of the Abell and ACO catalogs of clusters for tracing large-scale structure. Sutherland (1988), Olivier et al. (1990) and Sutherland & Efstathiou (1991) suggest the impact of redshift-angular separation anisotropies due to projection effects in the visually selected Abell catalog is severe. Struble & Rood (1991a) show that such effects are small ($\sim 3\%$) among the 1682 clusters in the ‘statistical sample’ subset of Abell’s catalog. Also, Postman, Huchra & Geller (1992) give a strong argument that the spurious structure due to projection

effects is insignificant in the sample of 351 Abell clusters with measured redshift that they present. On the other hand, Efstathiou et al. (1992) find significant indications of artificial anisotropies in the Postman et al. sample and show that the clusters selected from the APM (automatic plate measurement system at Cambridge University) galaxy catalog have no such anisotropies. Bahcall & West (1992) counter with another analysis, comparing Abell cluster results directly to the APM work, which indicated little effect from projection for the Abell clusters. Recently, Miller et al. (1998) also use newly-expanded samples of Abell and ACO $R \geq 1$ clusters with measured redshifts to show that anisotropies in the catalogs are on the same order as in the APM catalogs and not significant for purposes of large-scale studies. The new sample of Miller et al. consists of a large number (291) of $R \leq 1$ Abell/ACO clusters, 96% complete to $m_{10} = 16.8$. This sample is comprised of 198 northern Abell clusters, (188 of which have more than one measured redshift, with most of these redshifts from the MX Northern Abell Cluster Survey of Slingend et al. 1998) and 91 southern ACO clusters (most of the redshifts from the ESO Nearby Abell Cluster Survey of Katgert et al. 1996).

During our first observing run (August 1994 at ESO), we concentrated on the most dense of the two supercluster candidates. The Aquarius candidate is well-outlined by a 10° box on the sky centered on $\alpha = 23^h.3$, $\delta = -22^\circ$ (upper left of the $10^\circ \times 45^\circ$ strip shown in Fig. 1). We first worked to complete observations of the previously unmeasured clusters in this smaller region, and during the second run (September 1995), covered the larger strip down to our magnitude limit of $m_{10} \leq 18.3$.

3. Observations and Data Reduction

The observations took place over nine nights in August 1994, May 1995 and September 1995. The observations were under conditions of good to adequate seeing ($0.5'' - 2.0''$)

and transparency. The instrument used was the MEFOS (Meudon-ESO Fiber Optic Spectrograph) mounted on the ESO 3.6m telescope. The grating-CCD combination used resulted in a dispersion of $170 \text{ \AA}/\text{mm}$ and a resolution of about 11 \AA . The wavelength range was chosen to be $3800 \text{ \AA} - 6150 \text{ \AA}$.

We collected approximately 15–20 redshift-quality spectra within a given cluster field per hour. Comparison frames of helium and neon were taken before each exposure for wavelength calibration. “Fiber flats” (continuum spectra) were also taken for use in determining the location of the spectra on the CCD images.

3.1. Data Reduction

The data was reduced in the IRAF² environment, utilizing standard IRAF routines as well as modified routines designed for Steward Observatory’s MX Spectrometer. The MX-specific routines were written by John Hill, Bill Oegerle, David Batuski and Kurt Slingsland. The 2-dimensional CCD images were bias-subtracted and the individual spectra were extracted after being located on corresponding ‘fiber flat’ (quartz lamp) exposures. A dispersion solution from each object’s comparison (helium-neon) frame provided the spectra wavelength calibrations. A sky subtraction was performed after averaging all the sky spectra from a given exposure and normalizing by the strength of the [OI] 5577 \AA night sky line.

A problem has been reported (Felenbok et al. 1997) with some of the MEFOS fibers having persistent offsets after wavelength calibration, resulting in shifts of $\sim 0.5 \text{ \AA}$ in the

²IRAF is distributed by the National Optical Astronomy Observatories, which is operated by the Association of Universities for Research in Astronomy, Inc. (AURA) under cooperative agreement with the National Science Foundation.

measured wavelength of the 5577Å night-sky line. We examined our data for this problem and found that seven of our object fibers did indeed have such large offsets. Therefore, the wavelength solutions for galaxies observed with those fibers were each shifted by the negative of the average offset that we measured for the fiber in question.

3.2. Cross-correlation

We used the IRAF task “fxcor” to perform our cross correlations. Each spectrum was first cross-correlated against template spectra of eight stars with high-precision published velocities (Maurice et al. 1984). Each of these template stars was observed with MEFOS, in single-fiber mode. The star spectra were cross-correlated against each other, and the resultant velocities were compared with published values. Adjustments to our calculated velocities were then made to better match the published values. These corrections were on the order of 10 – 15 km s⁻¹ and were made to reduce errors in the star template velocities due to night-to-night instrument variations.

For an alternate determination of each galaxy’s velocity, a bootstrap technique was used. That is, the galaxy spectra were also cross-correlated against 20 low-redshift galaxy templates also observed on MEFOS (chosen for their high signal-to-noise ratio). The velocities of these galaxy templates had been previously determined through cross-correlation with the eight star templates mentioned above. In cases of high redshift object spectra ($z > 0.1$), the galaxy templates often provided a much more reliable velocity determination due to the greater number of comparable lines between the spectrum of the object and that of the template.

Each cross-correlation returned a heliocentric velocity and a cross-correlation strength (Tonry & Davis (1979) R value). For a particular target object, the set of calculated

velocities (20 when the galaxy templates were used, or eight when the star templates were used) was then weighted by $(R + 1)^2$ and averaged. Velocity errors were estimated using the $\sigma_v = Q/(R + 1)$ method of Hill & Oegerle (1993) and Pinkney et al. (1993). Q_{MEFOS} was determined from a selection of 22 galaxies that were each observed with MEFOS on two different occasions. The variations in these velocities were directly calculated, resulting in an average value of $Q_{MEFOS} = 260 \text{ km s}^{-1}$. Each of the measured velocities was then assigned an error of $\sigma_v = 260/(R + 1)$, where R is now an average value (over the successful cross-correlations with the eight star templates or the 20 galaxy templates.) To avoid unreasonably small errors for galaxies with R values greater than 13, we established a minimum error of 20 km s^{-1} . This lower limit allows for wavelength calibration and other errors in our system, and the magnitude of the minimum error was estimated from the scatter in measurements of the 5577\AA night-sky line, mentioned in subsection 3.1 above.

The results from the star template and galaxy template cross-correlations for each object were then compared. Cases that did not meet our minimum requirements ($R > 2.5$, median absolute deviation (MAD) of the velocities found for a galaxy $< 250 \text{ km s}^{-1}$, and a minimum of more than half of the templates cross-correlating successfully with the spectrum of the target) were discarded. For cases where a reliable redshift was determined from both the star template and the galaxy template cross-correlations, a comparison was made between the two sets of correlations, considering R , MAD, and the number of matched templates to determine which $(R + 1)$ -weighted velocity was more reliable. In most cases the velocity from the star template cross-correlation matched the velocity of the galaxy templates cross-correlation to within $1 \sigma_v$. In the rare instances where these two determinations did not agree, a visual inspection of the galaxy spectrum was used to determine which, if either, of the $(R + 1)$ -weighted velocities was correct. All of the spectra for the galaxies listed were examined visually to ensure that the velocities obtained were not occasionally the results of fluke occurrences in the data.

3.3. Emission Line Redshifts

All of our sky-subtracted galaxy spectra were examined for emission lines. If any reasonably likely candidate lines were found in a spectrum, the redshift of the galaxy was calculated using the `rvsao.emsao` package provided by the Smithsonian Astrophysical Observatory Telescope Data Center as an add-on to IRAF. If a galaxy had two or more apparent emission lines, all the good (not distorted by cosmic ray strikes, too low signal-to-noise, etc.) lines were used in `emsao` for the calculation. If only one emission line was found, and an absorption line velocity had been obtained that was in rough agreement with the emission line velocity, the single line velocity was accepted. A single emission line velocity was also considered acceptable even when the absorption line velocity for a galaxy was not deemed good enough for publication, if there were absorption features in good agreement with the location of the emission line.

The `emsao` task calculates a mean velocity by weighting the velocities returned by each emission line fit where:

$$W_i = \frac{\frac{1}{dvel_i^2}}{\sum \frac{1}{dvel_i^2}} \quad (2)$$

where $dvel_i$ is the error in the fit of the emission line with an RMS dispersion of $.05\text{\AA}$. `Emsao` returns similarly weighted errors. In addition to the line fit errors, we have found a 16 km s^{-1} root mean square variation when comparing the 5577\AA lines locations (see Section 3.1). Total errors in the emission line velocities were calculated by the root sum square of the error in the line fit and this inherent scatter (in the night-sky line wavelengths) due to the instrument. For the few galaxies where only the OII_{3727} was detected, a third systematic error was added because of the lower accuracy of the wavelength calibration towards the blue end of the spectra. This additional error was determined to be 22 km s^{-1} by comparing the velocity determination using only the OII_{3727} line with the velocity using multiple lines. We used 18 galaxies with multiple emission lines, that included OII_{3727} , for

the calculation of this third error.

4. Results

The recession velocities of all the galaxies observed in this program are presented in Tables 1, 2, and 3. Table 1 lists the results for galaxies in the MEFOS fields of clusters in the 10° square region of sky centered on $\alpha = 23^h.3, \delta = -22^\circ$, the heart of the Aquarius supercluster candidate. Table 2 gives the galaxy data for the clusters in the remainder of the target strip shown in Fig. 1. Table 3 presents the results for another supercluster candidate (Grus-Indus) that we had the opportunity to observe. The first two columns in each of these tables are the right ascension and declination coordinates (J2000) of the galaxies observed. Column 3 contains the $(R + 1)$ -weighted heliocentric velocities, and Column 4 of each table lists the estimated errors (σ_v). The last column has an object number entered if the subject galaxy has an emission line velocity (for cross-reference to Table 4). Velocities and errors given in Tables 1, 2, and 3 were calculated from the absorption lines in the spectra, unless there is an entry in the last column (Emission Reference) that ends with the letter ‘e.’ In those cases, the emission line velocity is listed in the Tables 1, 2 or 3. Entries in the last column that end with the letter ‘a’ indicate that an emission line velocity was determined (and is listed in Table 4), but the absorption line velocity is listed in the Tables 1, 2 or 3 and was used in our subsequent study of structure in the region.

Table 4 lists the emission line velocities for all our target galaxies that had acceptable emission lines. The first column indicates the Abell/ACO cluster, while the second column lists the reference number from Column 5 in Tables 1, 2 and 3. The third and fourth columns list the emission line velocities and estimated errors. The fifth column indicates which lines were detected in the spectrum. Lines within parentheses were seen, but not used in the velocity determination.

We obtained 737 redshifts in 46 cluster fields in our program. Thirty-nine of those cluster fields were in our $10^\circ \times 45^\circ$ strip. Nineteen additional $R \geq 1$ clusters in the strip had previously been observed, including three by Batuski et al. (1995) and eight with a single redshift per cluster by Ciardullo et al. (1985). The velocities of these clusters are presented in Table 5. Tables 5a, 5c and 5d list the Abell/ACO cluster number in column one. The mean and standard deviation are in columns two and four. Columns three and five labeled C_{BI} and S_{BI} , correspond to the bi-weight estimate of the data’s central location and scale (dispersion) respectively. These estimators were calculated using the ROSTAT statistical analysis package developed by Beers, Flynn & Gebhardt (1990). All velocities reported have been corrected for heliocentric motion. The final column indicates the number of galaxy redshifts that went into the velocity determinations. Table 5b lists fourteen clusters that are in the 10° square containing the Aquarius supercluster, but observed by other researchers.

Insufficient data were collected on clusters A2641, A3842, and A3861 to make a velocity determination. Clusters A3725 and A3944 were determined not to be clusters at all, but simply many galaxies strung out along the line of sight. These two clusters have been dropped from our sample, although, since A3725 has $m_{10} = 18.5$, it did not affect our level of completion within the strip.

Mean cluster velocities for the observed Abell clusters in this program have been determined with a procedure that has grown from a compilation of ideas of previous investigators (e. g., Batuski and Burns, 1985a, Postman, Huchra & Geller, 1992, Slingsland 1996). The data for each cluster field was examined for a grouping of four or more galaxy velocities with no gaps greater than 900 km s^{-1} , to serve as a starting point for an iterative membership determination. These velocities were used to calculate the classical mean and standard deviation, as well as a bi-weight location and scale of the cluster. These locations

and scales were determined using the ROSTAT package (Beers, Flynn, & Gebhardt, 1990). After the mean and standard deviation were calculated, any galaxies of the initial grouping that did not fall within 3σ of the mean velocity are excluded from cluster membership for the next iteration of the classical statistics calculation. Likewise, data points just on the other side of a 900 km s^{-1} gap were added for the calculation, as long as they did not fall outside 3σ from the (newly recalculated) mean velocity. In some cases, there are simply too few galaxy velocities in the cluster to do a statistical analysis. When $N = 3$ (and even $N = 2$ in the case of A3205, where cluster membership, based on relative distance from the projected cluster center, appeared very likely), only a simple mean is calculated from galaxies that fall within a $\pm 3000 \text{ km s}^{-1}$ grouping. In these cases, the calculated mean should be interpreted with caution.

In general this program did not observe Abell clusters for which redshifts had been previously measured. However, most of the previously-measured clusters within the Aquarius region have only a single measured redshift, and four of these were observed in our program for comparison, as well as confirmation of the redshifts. A2547, A2548, A2555, A2556 were studied by Ciardullo et al. (1985) at CTIO and observed again for this paper. These four were chosen because they constitute two pairs with small angular separation and each pair could be observed during a single exposure. Note that different galaxies were measured for this program than the ones measured by Ciardullo et al. The velocities for A2547, A2548, and A2556 that were determined by Ciardullo et al. (1985) were each well within the typical dispersion of Abell clusters (about 750 km s^{-1} , see for example, Zabludoff, et al. 1990) of the mean velocities calculated from our observations. On the other hand, Ciardullo et al. (1985) determined a velocity for A2555 of 41550 km s^{-1} by measuring one redshift and we obtained a mean cluster velocity of 33110 km s^{-1} , based on three galaxy redshifts.

4.1. The Aquarius Superclusters

One of the particular supercluster candidates (located in Aquarius) we investigated in the August 1994 and September 1995 ESO runs is one that was originally identified by Ciardullo et al. (1985). Ciardullo et al. identified the supercluster candidate via a “friends of friends” percolation scheme very similar to the one discussed in Section 2. They then measured single redshifts for 20 $R \geq 0$ Abell clusters in this region of sky and, from their results, concluded that there was no supercluster, only a chance projection of clusters along the line of sight out to $z \leq 0.2$. However, as pointed out earlier, measuring only a single redshift is dangerous, particularly in a region of such high surface density. We similarly (via percolation, see Section 2) identified a more extended version of the same supercluster candidate. Our identification included 39 clusters, 20 of which were originally identified by Ciardullo et al. (1985). The additional clusters from our analysis were, in projection, apparently farther outside the densest clump of clusters in Fig. 1 than the targets of Ciardullo et al. (1985).

The major finding to emerge in our analysis of this data is the confirmation of the presence of two extremely large and dense superclusters in Aquarius. Fig. 2a is a wedge plot of the redshift distribution for all $R \geq 1$ clusters that now have at least one measured redshift within our $10^\circ \times 45^\circ$ strip of the sky. The triangles and circles in this figure represent the clusters with $m_{10} \leq 18.3$ (on the ACO scale, which, largely because of the different media used, differs from the Abell 1958 magnitude scale), which are 87% complete, with 41 out of 47 clusters measured. The circles indicate clusters with a single measured redshift. The crosses in this figure are a few fainter clusters that had redshifts in the literature or that we observed because more time was available each night for the ends of the strip. Asterisks in this plot represent $R = 0$ ACO clusters with measured redshifts. As mentioned below, several of these $R = 0$ clusters were classified as $R \geq 1$ in Abell (1958).

Fig. 3 is the same as Fig. 2, except that $R = 0$ clusters are not plotted and Abell/ACO catalog numbers have been added.

The region from $cz = 24000$ to $cz = 36000$ km s⁻¹ (an extent of $\sim 110h^{-1}$ Mpc) around $\theta = 10^\circ$ in Fig. 3 contains 14 Abell/ACO clusters that percolate into a single structure with a percolation parameter of length $b = 25h^{-1}$ Mpc, which corresponds to a spatial number density of clusters, n , that is eight times the average spatial number density of ACO clusters, \bar{n} (see Section 2). In a percolation analysis at this density threshold of all the Abell/ACO $R \geq 1$ clusters with measured redshifts (similar to that of Bachall & Soniera 1984 and Batuski & Burns 1985a, but including redshifts from Slingsend et al. 1998, Katgert et al. 1996 and other sources in the literature), this was the structure of greatest extent that appeared. It was also one of the two structures with the largest number of member clusters. The Shapley Concentration percolates at this density to also include fourteen $R \geq 1$ clusters with an extent of only $56h^{-1}$ Mpc, while Corona Borealis becomes a complex of ten clusters with a $60h^{-1}$ Mpc extent. Two other supercluster complexes, each with six member clusters, have longest dimensions of $60h^{-1}$ Mpc in this analysis, and one structure (discussed below) consists of nine clusters in a $75h^{-1}$ Mpc filament. We note also that the Perseus-Pegasus supercluster filament (Batuski & Burns 1985b) and several other previously identified superclusters did not show up in this analysis since they are composed of a substantial number of $R = 0$ clusters.

The value of $n = 8\bar{n}$ is essentially the minimum value within the supercluster, since it corresponds to the value of the percolation length that connects the structure through its sparsest regions. The average density of this supercluster can be estimated by calculating the volume in a near-rectilinear box that encloses all the 14 clusters within their extremes of α , δ , and z . Such a box has a density that is a factor of 20 times the average $R \geq 1$ ACO cluster spatial number density.

Of the 14 clusters in the filament, four (listed in Table 5b and identified with open circles in Figures 2a and 3) still have only a single measured redshift, and as we mentioned in Section 1, this increases the risk of problems due to projection effects. However, only two of these single-redshift clusters, A2528 and A2541, are in ‘bridging’ locations within the Aquarius filament, such that new, significantly revised redshift information would cause substantial break-up of the percolated filament at $b = 25h^{-1}$ Mpc. With about 14% of Abell clusters with single reported redshifts turning out to have substantially revised redshifts after multiple measurements (see Section 1), there is thus a roughly 25-30% chance that additional observations will have large negative impact on the filamentary structure we report here. On the other hand, the region would still contain an unusual amount of superclustering (and if a cluster’s redshift is revised, it is still quite likely to be part of that structure given the line-of-sight nature of things in this region). Additionally, there are six single-measurement clusters in Table 5b that do not currently appear to be part of Aquarius, and about 20 fainter clusters with no measurements that could be found to occupy or extend this filament upon further observation.

There is an especially tight knot of six clusters in the region near $cz = 33000$ km s^{-1} and $\theta = 10^\circ$ in Figs. 2a and 3 (clusters A2546, A2553, A2554, A2555, A2579, and A3996). These clusters percolate with $b = 15.7h^{-1}$ Mpc ($n = 32\bar{n}$), and without A2553, the remaining five hold together at $b = 12.5h^{-1}$ Mpc ($n = 64\bar{n}$). If their redshifts are directly translated into distance according to Equation (1), this group of five occupies a sphere with radius $10h^{-1}$ Mpc (allowing sufficient room for the clusters to ‘fit’ by adding $2 h^{-1}$ Mpc to the minimum radius that would barely contain the apparent cluster center positions). The sphere would then have a spatial number density about 150 times the average for $R \geq 1$ ACO clusters, an amazing result, comparable to the five-cluster, densest portion of Corona Borealis supercluster (Postman, Huchra & Geller 1986), which is about $100\bar{n}$, and the nine $R \geq 1$ clusters of the Shapley Concentration (Scaramella et al. 1989) that percolate at

$b = 10h^{-1}$ Mpc to have $\sim 110\bar{n}$ for a similar spherical volume.

Only one of the clusters in the Aquarius knot, A2546, is limited to a single measured galaxy redshift, so high confidence can be placed on the reality of this extreme density peak (as is also the case for the three other peaks discussed above). Note also that A2548, an $R = 0$ cluster that was included on our list of targets because it could be observed in the large MEFOS field at the same time we were observing A2547, also happens to have a redshift that places it in the knot, contributing further to the density of the region. A2548 had been classified $R = 1$ by Abell (1958).

On the high redshift end of the Aquarius filament, four $R = 0$ (by ACO criteria) clusters are in positions that bridge gaps at $b = 30h^{-1}$ Mpc (see the asterisk symbols in Fig. 2a), further extending the structure to a total length of $150 h^{-1}$ Mpc, by connecting in the $R \geq 1$ clusters A2521, A2547, A2550, and A2565. Three of these clusters, A2518, A2540, and A2542, had been classified as $R = 1$ in Abell’s catalog and were reclassified as $R = 0$ in ACO. The other cluster, A2568, is classified $R = 0$ in both catalogs. Redshifts for all four of these clusters were measured by Ciardullo et al. However, since the $R = 0$ cluster redshifts are very incomplete in this region (for instance, only five out of 16 measured in the $10^\circ \times 10^\circ$ square of sky around the projected Aquarius filament), no analysis of the significance of their contribution to the structure in the region is appropriate at this time.

There is another collection of nine ACO/Abell $R \geq 1$ clusters that percolates at $b = 25h^{-1}$ Mpc ($n \sim 8\bar{n}$) across the foreground in the region of the Aquarius supercluster. The member clusters are A2456, A2480, A2492, A2559, A2569, A2638, A2670, A3897 (also listed as A2462 in Abell 1958), and A3951. Since A2670 is near the Aquarius-Cetus boundary, we will hereafter identify this supercluster as Aquarius-Cetus, to distinguish it from the Aquarius supercluster discussed above. The wedge plot in Fig. 4 is centered on the dashed line in Fig. 1, and with its 12° width, it covers both of the superclusters in this

region. The clusters of the Aquarius supercluster are identified with filled circular symbols, while Aquarius-Cetus clusters are filled triangles. Open triangles stand for clusters that do not percolate into either supercluster at $b = 25h^{-1}$ Mpc. The Aquarius-Cetus complex spans an overall distance of $75 h^{-1}$ Mpc, and it also has an especially high-density group of four clusters (A2456, A2480, A3897, and A3951), with an average density (sphere-average method above) of $70\bar{n}$. All four of these clusters have multiple measured redshifts.

At the relatively low density threshold of $n \sim 4\bar{n}$, the Aquarius and Aquarius-Cetus superclusters percolate together, through the crossing of the gap between A2538 and A3951.

Another approach to analyzing our redshift data for the Aquarius region is to consider our observations as 1° wide pencil-beams sampling this small region of the sky in several spots (especially since one is compelled, with the large field and the mechanical arms of MEFOS, to choose several target galaxies per field that are well away from the apparent cluster center). We can then view the aggregate velocity distribution of the galaxies observed in this region with histograms (Figures 5 and 6). As one might expect from the above discussion of the knot of six clusters, Fig. 5 shows a large peak at ~ 33000 km s^{-1} . However, when the velocities associated with the clusters in each of our fields are subtracted, we have the result in Fig. 6, which shows a sizeable (about 20 galaxies) peak in the velocity distribution remains at ~ 33000 km s^{-1} . This suggests that several of the fields targeted toward other clusters might be sampling a more extended ‘background’ population around the six cluster knot (as well as another population around 26000 km s^{-1}). The 2dF survey of this region should confirm whether or not such extended structure exists around the knot of clusters.

We also point out that the percolation analysis of $R \geq 1$ Abell/ACO clusters with measured redshifts adds a seventh cluster (A3677) to another high-density (percolating at $b = 12.5h^{-1}$ Mpc) supercluster in Microscopium identified by Zucca et al. (1993) as

consisting of six measured-redshift $R \geq 1$ clusters (A3682, A3691, A3693, A3695, A3696, A3705). Each of these seven clusters has many measured redshifts from Katgert et al. (1996). Fitting of a sphere around the five of these clusters that percolate at $b = 10h^{-1}$ Mpc results in $n = 130\bar{n}$. Of course, the densities calculated by this sphere-fitting algorithm may differ considerably from the actual spatial densities of the clumps considered, if there is much of a peculiar velocity/dynamical component to the redshifts of the clusters (see section 4.3 below), but treating these apparent peaks in the same way allows for a rough estimation of their comparative densities. Thus, including Shapley and Cor Bor, we have four very high density peaks, each involving at least five rich clusters, within $z \leq 0.11$.

4.2. Significance of the Superclustering in Aquarius

We took two approaches to evaluating the statistical significance of the Aquarius supercluster filament. Both of these involved analysis of simulated ‘universes’ of point locations in space corresponding to the centers of pseudo-clusters of galaxies with two-point spatial correlation functions very similar to that of the $R \geq 1$ Abell clusters. Following the procedure of Batuski & Burns (1985b), which was based on the hierarchical nested-pairs technique of Soneira & Peebles (1978), one hundred catalogs of pseudo-clusters were created by placing pairs of pairs within a spherical volume in such a manner that $\xi(r)$ closely matched that of the recently enlarged sample of Abell clusters with redshifts analyzed in Miller et al. (1998), as shown in Fig. 7. This procedure can be visualized as placing a ‘long rod’ at a random point in space with a random orientation, then at each end of the rod placing a short rod, again with random orientation, and finally placing a cluster at each end of each short rod, dropping any clusters that were outside the radius of the spherical volume of the simulation. The lengths of the rods were governed by

$$\Lambda = A(1 - Bx^\alpha), \quad (3)$$

where $A = 22h^{-1}$ Mpc and $B = 0.5$ for the long rods, $A = 11h^{-1}$ Mpc and $B = 0.96$ for the short rods, $\alpha = 1.5$ for both cases, and x is a uniformly distributed random number between 0 and 1. Finally, 25% of the points generated with this algorithm were randomly selected for deletion from the models so that $\xi(r)$ on small scales ($5 - 10 h^{-1}$ Mpc) closely follows the Abell/ACO case and so that the ratio of triple-cluster clumpings to double-cluster clumpings (about 7:1) could begin to approach that observed in the Abell/ACO catalogs (about 3:1) at $b = 25h^{-1}$ Mpc. These simulations thus have large-scale clumping very similar to that of the Abell/ACO clusters but no particular tendency to form filamentary structures, since the spatial orientations of all the pairs were determined randomly (uniform in ϕ in the $x - y$ plane and uniform in $\cos\theta$ for the angle with the z -axis).

4.2.1. Two-dimensional Density Peaks

We first examined each of the 100 pseudo-cluster catalogs from the central position within its spherical volume of space to find peaks in the projected 2-D number density of clusters on the ‘sky’ of an imagined observer at the center of such a universe. In the $10^\circ \times 10^\circ$ square of sky centered on the densest part of the Aquarius supercluster ($\alpha = 23^h.3, \delta = -22^\circ$), there are 23 $R \geq 1$ Abell/ACO clusters to a depth of $400 h^{-1}$ Mpc, only one of which has an unmeasured redshift (estimating the redshift from the ACO $m_{10} - z$ relation, the $400 h^{-1}$ Mpc limit corresponds to an ACO magnitude limit of $m_{10} < 18.3$ and an Abell magnitude limit of $m_{10} < 17.6$). This is the most pronounced peak surface density of measured and unmeasured $R \geq 1$ clusters to this depth on our sky. One might think that part of this effect is the result of this region being so complete in redshifts, but even counting more deeply, using 500 Mpc or 600 Mpc as the cutoff, beyond

which distances there are few clusters with measured z so that effectively there is only a uniform magnitude limit, this peak remains the highest in our sky by at least 15%.

In the 100 psuedo-cluster simulations, surface density peaks of similar amplitude (22 - 25 clusters in a 10° square) were identified on the ‘sky’ of our central observer, and then the clusters within that square were checked to see how often they would percolate, with $b = 25 h^{-1}$ Mpc, into a structure of length $100 h^{-1}$ Mpc or greater. This happened in about 1% of the peak-surface-density cases, so having such a long structure roughly along the line of sight is a two sigma event in a population of pseudo-clusters that are clumped in a scheme that closely approximates the two-point correlation function of rich Abell clusters but avoids the introduction of more than chance filamentation. This result suggests that finding such a structure as the Aquarius filament through the observational approach that we used is very unlikely unless rich clusters in the real universe are more commonly members of filamentary supercluster structures in comparison to the pseudo-clusters in the simulations.

4.2.2. *Ellipsoid Fitting*

In the second analysis of the significance of the Aquarius supercluster, we first fit a triaxial ellipsoid through the 14 member cluster positions, using the technique of Jaaniste et al. (1998). The resulting ellipsoid had axes ratios of 4.3:1.0:0.70, with the long axis tilted at 6.9° from the line of sight. For examining filamentation in the Abell/ACO catalogs and the 100 pseudo-cluster catalogs, we chose to classify as filaments supercluster ellipsoids with a long axis at least three times the length of the longer of the other two axes (axis ratio of $R_A \geq 3.0$), so that such identified filaments could have some substantial curvature as well as one axis that was clearly much longer than the others.

The Abell/ACO sample that we examined for filamentation includes all $R \geq 1$ clusters

with galactic latitude at least 30° from the galactic plane, measured redshifts, and distances less than $300 h^{-1}$ Mpc, using Equation (1). The sample includes 50 new cluster redshifts soon to be published in Miller et al. (1999). The distance cutoff was chosen because Miller et al. (1998) show that the $R \geq 1$ Abell clusters north of $\delta = -17^\circ$ and the $R \geq 1$ ACO clusters south of that declination each have a relatively flat spatial number density distribution out to $z = 0.10$ before it drops off steeply, indicating that redshift coverage is quite complete within $D \sim 300h^{-1}$ Mpc. In this sample of 370 clusters, using a percolation length of $b = 25h^{-1}$ Mpc, as we used above for defining the Aquarius and Aquarius-Cetus superclusters, there are 64 superclusters (with two or more member clusters), 14 of which having five or more members. One of these superclusters consists of six of the clusters found to be members of the Aquarius supercluster (the other eight Aquarius member clusters are more distant than $300h^{-1}$ Mpc and were thus excluded from the sample), and another is Aquarius-Cetus.

When we fit ellipsoids to the superclusters with five or more members ($N_c \geq 5$ at $b = 25h^{-1}$ Mpc), only three among these 14 superclusters satisfied our definition of a filament: Ursa Major (with $N_c = 5$) had $R_A = 4.7$, Virgo-Coma ($N_c = 6$, none of which is the Coma Cluster) had $R_A = 3.2$, and Aquarius-Cetus ($N_c = 8$) had $R_A = 3.0$. Ursa Major runs closest to the line of sight, with a tilt of only 14° , while Virgo-Coma and Aquarius-Cetus are tilted 68° and 73° , respectively. The ellipsoid fit to the fragment of the Aquarius supercluster that lies within $D = 300h^{-1}$ Mpc had $R_A = 2.5$, so it did not qualify as a filament.

We then searched for filaments in fifty catalogs of pseudo-clusters with $\xi(r)$ constrained to approximate that of Abell/ACO clusters. Limiting these catalogs to the same distance and galactic latitude ranges as the Abell/ACO case above, there were an average of 440 pseudo-clusters per sample. This number is somewhat greater than the 370 Abell/ACO

clusters in our sample, primarily because we chose to use the average space number density of ACO clusters ($\sim 8 \times 10^{-6} h^3 \text{ Mpc}^{-3}$) throughout these pseudo-cluster catalogs rather than the density of Abell clusters ($\sim 6 \times 10^{-6} h^3 \text{ Mpc}^{-3}$, Miller et al. 1998) or an average of the two densities. We chose the ACO density because we have been using ACO criteria throughout the characterization of the Aquarius supercluster. We also point out that the parameter of interest here is the *fraction* of $N_c \geq 5$ superclusters that have $R_A \geq 3.0$, which is not affected by a small change in density.

With $b = 25h^{-1} \text{ Mpc}$, each of the pseudo-cluster catalogs percolated an average of 7.7 superclusters with five or more members, and 20% of these superclusters satisfied the $R_A \geq 3$ definition of a filament. (For reference, the same analysis of 100 catalogs of entirely random cluster positions yielded 0.64 $N_c \geq 5$ superclusters per catalog, 19% of which were filamentary, indicating that our pseudo-cluster creation algorithm did indeed not introduce extraneous filamentarity.)

The surprising conclusion to this analysis is that even though filamentary arrangements of galaxies and clusters of galaxies (generally including $R = 0$ clusters) have commonly been reported in observational studies of large-scale structure (*e. g.*, Batuski & Burns 1985b, de Lapparent et al. 1988 and 1991, Giovanelli & Haynes 1993, da Costa et al. 1994) and even though this one region of the sky in Aquarius contains two pronounced filaments of rich clusters, the large and nearly complete sample of $R \geq 1$ Abell/ACO clusters actually shows no more filamentation than what could be expected by chance alignments in a clumpy universe. While the Abell/ACO sample contains a much higher number of large ($N_c \geq 5$) superclusters than the average pseudo-cluster catalog (14 versus 7.7), essentially the same fraction of such superclusters in either case (21% for Abell/ACO and 20% for pseudo-clusters) satisfy $R_A \geq 3$. For $b = 20$ and $30h^{-1} \text{ Mpc}$, and for $R_A \geq 2$ as well as $R_A \geq 3$ for the filamentation threshold, the Abell cluster sample also showed similar

amounts of filamentation to that seen in the pseudo-cluster catalogs.

We thus appear to have a contradiction between our results in this section and the finding of the previous section. That earlier finding indicated a low probability that the projected density enhancement on the sky in Aquarius would turn out to contain such an elongated structure as the Aquarius filament unless there is significant filamentation among Abell clusters. The Abell/ACO sample shows no such filamentation.

4.3. Dynamics of the Aquarius Knot

Knowledge of the masses and dynamical states of the superclusters discussed in this paper are significant to the study of the mass distribution on large scales in general. The entire Aquarius and Aquarius-Cetus filaments each have spatial extents that imply crossing times that are a few times the Hubble time (assuming peculiar velocities of $\sim 1000 \text{ km s}^{-1}$ – see discussion below), so these structures can not have broken away from the Hubble Flow and may well not be gravitationally bound overall. Until they have been studied in far more detail, little can be said about dynamics within such extended structures. However, the knot within the Aquarius filament is dense enough and has sufficient redshift information available to warrant a closer look now. The same is true of the newly-identified Microsopium Supercluster, which we will also examine in this section.

The knot within the Aquarius supercluster is comparable in density enhancement to the Shapley Concentration and the Corona Borealis (Cor Bor) superclusters (see Section 4.1). However, Tables 5a and 5b show how sparsely the region has been sampled thus far. While most of the clusters observed for this program have enough galaxy redshifts for reliable cluster velocity determinations, none have enough for accurate velocity dispersions, which are needed for reasonable cluster mass determinations.

Recent work by Small et al. (1998) has shown that both the virial mass estimator and the projected mass estimator (Bahcall & Tremaine 1981) give reasonable mass estimates for clusters with ~ 30 or more galaxy observations. Small et al. (1998) determined a mass for Cor Bor of at least $3 \times 10^{16} h^{-1} M_{\odot}$ and a mass-to-light ratio of $726 h(M/L)_{\odot}$. The small number of galaxies measured for our initial observations prohibits a similar determination of mass for the Aquarius superclusters. At best, a simple sum of the ‘typical’ masses of Abell clusters would give a lower limit to the total mass. Since both filaments discovered contain some clusters with single measured redshifts, only the knot within Aquarius has enough clusters with velocity dispersions for estimates (although rather rough given the small number of redshifts available for most of these clusters) of individual cluster masses. Thus, assuming A2546 and A2555 to be typical Abell/ACO $R \geq 1$ clusters with $\sigma_v \sim 800 \text{ km s}^{-1}$ (like A2553, A2579, and A2554, which according to Zabludoff et al. 1990 has $\sigma_v = 827 \text{ km s}^{-1}$ and for which Girardi et al. 1998 determined a cluster mass of $6.4 \times 10^{14} h^{-1} M_{\odot}$), we estimate each to have a cluster mass $\sim 7 \times 10^{14} h^{-1} M_{\odot}$ and find a total lower-limit mass for the knot $\sim 6 \times 10^{15} h^{-1} M_{\odot}$ (about half of the mass coming from the large dispersion of A3996). A mean harmonic radius of $1.5 h^{-1} \text{ Mpc}$ was assumed for each virial-theorem estimation, since that was the average projected distance from the cluster center of the cluster members observed. Similar calculations using the velocity dispersions reported by Katgert et al. (1996) for clusters of the Microscopium supercluster result in a lower-limit mass of $\sim 4 \times 10^{15} h^{-1} M_{\odot}$ (Girardi et al. 1998 estimate a total mass of $2 \times 10^{14} h^{-1} M_{\odot}$ for three of the seven clusters). We note that the sum of the masses of the clusters in Cor Bor as determined by Small et al. (1998) in the same manner is $5.3 \times 10^{15} h^{-1} M_{\odot}$, which is a factor of 6-8 smaller than their mass determinations by the virial mass estimator or the projected mass estimator.

It may soon become feasible to conduct a study of the dynamics among these clusters to further constrain the mass of the system. The 2dF redshift survey of this region, already

underway, should provide a large number of redshifts for galaxies within and between clusters in the knot (as well as for the rest of the supercluster). However, another large observational program, employing a secondary distance indicator that can provide distances of sufficient accuracy, will be necessary to determine cluster peculiar velocities in the region. The clusters in the knot have a radial distance range of about $13 h^{-1}$ Mpc (using their redshifts directly), at an average distance of about $325 h^{-1}$ Mpc, so one would need accuracies of only a few percent from the secondary indicator. Some standard-candle-type analyses that might apply at such distances, such as brightest (or third- or tenth-brightest) cluster galaxies, or even entire cluster luminosity function analyses as attempted by Small et al. on Corona Borealis, are sufficiently coarse that they are unlikely to ever provide the accuracy needed for a study of dynamics within the knot. Other methods, such as approaches using relations like Tully-Fisher or those employing Type I supernovae, hold the promise of achieving the necessary accuracy when large amounts of observational data become available for their application.

We can at the present time get a rough conception of the dynamics of the Aquarius knot and Microscopium by looking at typical supercluster crossing times and virialization timescales and by applying a technique Sargent & Turner (1977) developed to measure the slowing of the Hubble flow for systems where only redshift information is known. One can calculate the angle between the separation vector and the plane of the sky at the midpoint between clusters using

$$\alpha = \arctan\left[\frac{1}{2}(z_1/z_2 - 1) \cot\left(\frac{1}{2}\Delta_{12}\right)\right]; \quad 0 \leq \alpha \leq \pi/2, \quad (4)$$

where $z_1 \geq z_2$ and Δ_{12} is the separation between clusters 1 and 2 on the sky in radians. If $\bar{\alpha} < 32.7^\circ$ the region is expected to have a slowed Hubble flow. If violent relaxation has not yet occurred, such system should appear flattened in the redshift direction. If $\bar{\alpha} > 32.7^\circ$

the region may have reached virial equilibrium and the system would appear elongated along the line of sight. If $\bar{\alpha} \sim 32.7^\circ$, its isotropic value, we expect an unperturbed Hubble flow or a system in the midst of relaxation. Using only a few clusters per supercluster for such calculations clearly will make for very large error bars, compared to studies of the dynamical states of clusters or groups of galaxies, but the results below can still provide some useful indications.

Postman et al. (1988) calculated $\bar{\alpha} = 56.5^\circ \pm 12.7^\circ$ for Cor Bor (with A2124 excluded from the analysis because of its apparently greater separation from the rest of the supercluster), a significant indication of virialization, although they noted that true spatial elongation rather than dynamical redshift-space elongation could easily be the major factor in the case of this one well-studied supercluster. The value of $\bar{\alpha}$ for the six-cluster knot within the Aquarius supercluster is $\bar{\alpha} = 28.8^\circ \pm 18.5^\circ$. Since this result is well within the errors (determined as in Wagner & Perrenod (1981)) of the isotropic result, the knot is clearly not significantly elongated or flattened along the line of sight. This suggests either that the supercluster has not yet significantly broken away from the Hubble expansion or that it has begun violent relaxation but is not yet virialized.

From the extent of the system on the sky, we expect the supercluster crossing time of a typical cluster with $v_{pec} \sim 800 \text{ km s}^{-1}$ (typical of many recent findings, *e. g.* Bahcall, Gramman & Cen 1994, Croft & Efstathiou 1994, but a bit high compared to $v_{pec} \sim 500 \text{ km s}^{-1}$ from Bahcall & Oh 1996) to be $T_c \sim 5 \times 10^9$ years, thus the Aquarius knot could be gravitationally bound. The virialization timescale for a spherically symmetric collapsing mass is (Gunn & Gott 1972)

$$T_v = \frac{2.14}{\sqrt{G\rho}} \tag{5}$$

where ρ is the current-epoch mass density. Postman et al. (1988) determined T_v for Cor

Bor to be $\sim 2 \times 10^{10}$ years, so they concluded that it was unlikely that the supercluster was virialized, although they found that the mass of Cor Bor was sufficient to bind the supercluster (as did Small et al. 1998). We would expect T_v to be about the same for the Aquarius knot, which has roughly the same rich-cluster spatial density as Cor Bor. These values of $\bar{\alpha}$, T_c and T_v for the knot do not allow for discrimination between the two cases of continued expansion with the Hubble flow and violent relaxation.

We also note that $\bar{\alpha}$, T_c and T_v are very similar to the values for the Aquarius knot for the seven clusters of Microscopium ($\bar{\alpha} = 31.7^\circ \pm 17.2^\circ$) and for the nine clusters of Shapley ($\bar{\alpha} = 34.3^\circ \pm 16.2^\circ$). Thus, of the four rich-cluster density peaks, none show noticeable flattening in the redshift direction, indicative of slowing expansion. Cor Bor has a $\bar{\alpha}$ value suggesting virialization (although this seems unlikely from other measures), while Aquarius, Microscopium, and Shapley have an isotropic appearance, but could possibly be in the process of relaxation, given the timescales involved. These results highlight the importance of further study of all four of these complexes of clusters. Much work has already been done on Shapley and Cor Bor, but the Aquarius and Microscopium peaks could provide new insight into large-scale dynamics in the universe.

4.4. The Other Targeted SCCs

The Eridanus SCC was also included in our target strip on the sky (Fig. 1). The clusters identified in the friends-of-friends analysis as likely members (A3802, A3817, A3818, A3820, A3834, A3841, and A3845) lie roughly along $\theta = 40^\circ$ in Fig. 2. However, the clusters near that line that we measured (A3820 and A3845 were not observed because they are slightly fainter than our magnitude limit of $m_{10} = 18.3$ in the strip) have widely differing redshifts (see Table 5c), and there is no indication of superclustering in that region. A3817 was observed previously (Batuski et al. 1995).

The redshift distribution that we found for the Grus-Indus SCC (seven clusters near $\alpha = 4^h$, also listed in Table 5d) is a bit more interesting, with three clusters, A3148, A3166, and A3171, within the range $32800 \leq cz \leq 37200 \text{ km s}^{-1}$. These clusters have spatial separations of 19 and $28 h^{-1} \text{ Mpc}$, suggesting superclustering, but with so few clusters involved there is no great statistical significance to their proximity. In 100 catalogs of pseudo-clusters distributed randomly in space to a distance of $400 h^{-1} \text{ Mpc}$ (about 1060 pseudo-clusters per catalog, with exclusion of a region bounded by a latitude limit of $\pm 30^\circ$ to simulate galactic obscuration), we found an average of 35 ‘superclusters’ per catalog consisting of three pseudo-clusters that would percolate at $b = 30h^{-1} \text{ Mpc}$. Only five superclusters of six or more points were found per catalog and a supercluster of 10 or more was only found in one out of five catalogs. Thus, with $\sim 10\%$ of clusters in 3-D groupings of three clusters, an observing program targeting apparent 2-D clumpings on the sky would have considerable likelihood of finding some superclusters of three clusters even if the spatial distribution of the clusters were entirely random. On the other hand, finding several more populous superclusters, as researchers have done, obviously requires a spatial distribution something akin to that represented by the two-point spatial correlation functions of Fig. 7.

5. Conclusion

The Aquarius supercluster appears to be a highly significant single structure of 14 $R \geq 1$ ACO clusters that percolates at $b = 25h^{-1} \text{ Mpc}$ ($n = 8\bar{n}$), and extends in a filamentary fashion at least $110 h^{-1} \text{ Mpc}$. This is the largest structure involving such rich clusters at such a density contrast that has been identified to date. With the inclusion of four $R = 0$ ACO clusters that were classed as $R = 1$ by Abell, the apparent filament can be traced to an extent of $150 h^{-1} \text{ Mpc}$, with 22 member clusters, at $b = 30h^{-1} \text{ Mpc}$. Aquarius is also the second most filamentary of the superclusters that percolate among the

measured- z , rich Abell/ACO clusters at $b = 25h^{-1}$ Mpc, having $R_A = 4.3$ for its ellipsoid fit.

The scale of this structure is similar to that seen in the Great Wall of galaxies (de Lapparent et al. 1988 and 1991) and in the Perseus-Pisces-Pegasus supercluster (*e. g.*, Gregory, Thompson & Tifft 1981; Haynes et al. 1988; and extended with primarily $R = 0$ clusters by Batuski & Burns 1985a). The lengths of all these structures are approaching 5-10% of the horizon length of the universe, the scale of many of the features observed by COBE in the cosmic microwave background (Smoot 1992).

Besides the extent and shape of Aquarius, the high-density peak that it contains is also of great interest. Our analysis of available redshift data for the clusters in this peak and the estimated time-scales involved leaves open the possibility that the grouping may have broken away from the Hubble expansion to be currently in collapse toward an eventual virialized state. Including the seven-cluster supercluster in Microscopium, four such large cluster overdensities are now known to exist within $z \leq 0.11$. These observations constrain the theoretical models for the formation of such structure, since simulations based on such models will need to generate similar numbers of high density peaks in the cluster distribution, with their sizeable impacts on statistics of large-scale structure like the two-point spatial correlation function, as illustrated by Postman et al. (1992) and Miller et al. (1998). Postman et al. found that Corona Borealis accounted for 20% of the power in $\xi(r)$ for their 156 $R \geq 1$ Abell cluster sample, while Miller et al. found that Cor Bor and Microscopium contributed $\sim 20\%$ to $\xi(r)$ in their sample of 289 $R \geq 1$ Abell/ACO clusters. These knots of clusters will no doubt also eventually help in the determination of Ω_\circ , once we have secondary distance indicators of sufficient accuracy.

The filamentary structure of the Aquarius supercluster may have even greater extent than what is reported here. As can be seen in Fig. 3, A2547 and A2550 lie just beyond

the high- z end of the filament, in position to extend the structure to a length greater than $200h^{-1}$ Mpc if other clusters (or galaxy bridges) are found to fill in the gaps upon future observation. There are another dozen clusters nearby on the sky (mostly fainter than the $m_{10} = 18.9$ limit that was reached for the small, $10^\circ \times 10^\circ$ region in the heart of the Aquarius clump, but a few with $18.3 < m_{10} < 18.9$, slightly farther away on the sky) that do not have measured redshifts. These should be observed soon to see if they might reveal more structure in the region.

We also report the discovery of the Aquarius-Cetus supercluster, another prominent filamentary structure among $R \geq 1$ Abell/ACO clusters, with its nine clusters percolating at $n = 8\bar{n}$ and its own apparent knot of four clusters. (Two of the cluster redshifts for this structure are based on single-galaxy measurements, however, and only one of those (A2638) is in a bridging position that might significantly affect the size and shape of the supercluster if its redshift is later corrected.)

The filamentary shapes of both the Aquarius and Aquarius-Cetus superclusters turn out to be unusual in the spatial distribution of $R \geq 1$ Abell/ACO clusters. Our analysis in section 4.2 revealed that, while the Aquarius region contains two clearly filamentary structures among such rich clusters, the Abell/ACO samples do not appear to have appreciably more filamentation than could be expected by chance within a population of objects with similar two-point correlation function. While poorer clusters and individual galaxies have been seen to follow filamentary patterns in many observational programs, the $R \geq 1$ clusters do not appear to participate in such patterns, at least for aggregates of five or more rich clusters. This result is in disagreement with the implication from our projected-filament-frequency analysis of Section 4.1 that significant filamentation would need to exist in the Abell/ACO sample in order for a near-line-of-sight filament of the extent of Aquarius to be largely responsible the two-dimensional density enhancement seen

in that part of the sky.

The superclusters in this extremely interesting region should be observed in a very thorough redshift survey of thousands of individual galaxies in the immediate vicinity. (Such a survey is now being conducted as part of the 2dF program (Jones et al. 1994)). This is desirable in order to get more velocities of cluster members in those cases where only one galaxy has been measured and also to look for bridging structure among the clusters, such as that found in Chincarini, Rood & Thompson (1981), de Lapparent et al. (1988 and 1991), Gregory & Thompson (1984), Gregory, Thompson & Tifft (1981), Tarenghi et al. (1979), Postman et al. (1988), Small et al. (1998), and other papers on previously-identified superclusters. The proximity and filamentary arrangements of so many rich clusters make the Aquarius and Aquarius-Cetus superclusters remarkable occurrences, but given our finding that superclusters of rich Abell/ACO clusters show no more than chance elongation, future observations should perhaps be expected to show the filaments to be a chance alignments of disconnected clumps of clusters, obviating any need for theoretical models to produce extensive filaments of rich clusters. The details of possible structure connecting the clusters will be important in determining their true significance for the purpose of modeling and understanding large-scale structure in the universe.

DJB, CM, and KAS were supported in this work by National Science Foundation Grant AST-9224350. KAS gratefully acknowledges Sigma Xi, the Scientific Research Society for a travel grant for the August 1994 run. CM is thankful for partial support through a fellowship from Maine Science and Technology Foundation (Grant MSTF 97-25) and the NASA EPSCOR program. DJB also wishes to thank the University of Paris 7 and Paris Observatory for partial support for this research effort. Support was also provided by CNRS through the Cosmologie GDR Programme.

The authors performed much of the work for this paper on workstations obtained

under an equipment grant from Sun Microsystems, Inc. to the University of Maine.

REFERENCES

- Abell, G. O. 1958, *ApJS* 3, 211
- Abell, G. O., Corwin, H. G., & Olowin, R. P. 1989, *ApJS* 70, 1 (ACO)
- Bahcall, N., Oh, S. 1996, *ApJ* 462, L49
- Bahcall, N., Gramman, M., & Cen, R. 1996, *ApJ* 436, 23
- Bahcall, N., & Soniera, R. 1983, *ApJ* 270, 20
- Bahcall, N., & Soniera, R. 1984, *ApJ* 277, 27
- Bahcall, N., & Tremaine, S. 1981, *ApJ* 244, 805
- Bahcall, N.A. & West, M.J. 1992, *ApJ*, 392, 419
- Batuski, D. J., & Burns, J. O. 1985a, *AJ* 90, 1413
- Batuski, D. J., & Burns, J. O. 1985b, *ApJ* 299, 5
- Batuski, D. J., Burns, J. O., Newberry, M. V., et al. 1991, *AJ* 90, 1413
- Batuski, D., Maurogordato, S., Balkowski, C., & Olowin, R., 1995, *A&A*, 294, 677
- Beers, T. C., Flynn, K. & Gebhardt, K. 1990, *AJ* 100, 32
- Broadhurst, T. J., Ellis, R. S., Koo, D. C., & Szalay, A. S. 1990, *Nature* 343, 726
- Chincarini, G. & Rood, H. J. 1979, *ApJ*, 230, 648
- Chincarini, G., Rood, H. J., & Thompson, L. A. 1981, *ApJ* 249, L47
- Ciardullo, R., Ford, H., & Harms, R. 1985, *ApJ* 293, 69
- Croft, R. & Efstathiou, G. 1994, *MNRAS*, 268, L23

- da Costa, L. N., Geller, M. J., Pellegrini, P. S., et al. 1994, ApJ 424, L1
- de Lapparent, V., Geller, M. J., & Huchra, J. P. 1988, ApJ 332, 44
- de Lapparent, V., Geller, M. J., & Huchra, J. P. 1991, ApJ 369, 273
- Dressler, A. 1988, ApJ 329, 519
- Dressler, A. 1991, ApJS 75, 241
- Efstathiou, G., Dalton, G. B., Sutherland, W. J., & Maddox, S. J. 1992, MNRAS 257, 125E
- Felenbok, P., Guerin, J., Fernandez, A., Cayatte, V., Balkowski, C., & Kraan-Korteweg, R.
1997, **Experimental Astronomy**, 7, 65
- Giovanelli, R., Haynes, M. P., 1993, AJ 105, 1271
- Girardi, M., Giuricin, G., Mardirossian, F., Mezzetti, M., & Boschin, W. 1998, ApJ 505, 74
- Gregory, S. A., & Thompson, L. A. 1978, ApJ 222, 784
- Gregory, S. A., & Thompson, L. A. 1984, ApJ 286, 422
- Gregory, S. A., & Thompson, L. A., Tifft, W. G. 1981, ApJ 243, 411
- Gunn, J. E., & Gott, J. R. 1972, ApJ 176, 1
- Haynes, M. P., Giovanelli, R., Starosta, B., & Magri, C. 1988, AJ 92, 250
- Hill, J. M., & Oegerle, W. R. 1993, AJ 106, 831
- Huchra, J., Davis, M., Latham, D., & Tonry, J. 1983, ApJS 52, 89
- Jaaniste, J., et al. 1998. A&A 336, 35
- Jones, A., Bland-Hawthorn, J., & Kaiser, N. 1994, BAAS 185, 56

- Katgert, P., et al. 1996, *A&A*, 310, 8
- Kirschner, R.P., Oemler, A., Jr., Schechter, P.L., & Schectman, S.A. 1981, *ApJ*, 248, L57
- Kirshner, R. P., Oemler, A., Jr., Schechter, P. L. & Shectman, S. A. 1987. *ApJ* 314, 493
- Maurice, E., et al. 1984, *A&AS* 57, 275
- Miller, C., Slingsend, K., Batuski, D., & Hill, J. 1998, *ApJ* Submitted.
- Miller, C., Batuski, D., Slingsend, K., & Hill, J. 1999 , *ApJ* In preparation.
- Olivier, S., Blumenthal, G., Dekel, A., Primack, J. R., & Stanhill, D. 1990, *ApJ* 356, 1
- Pinkney, J., Rhee, G., Burns, J., Hill, J., Oegerle, W., Batuski, D., & Hintzen, P. 1993, *ApJ* 416, 36
- Postman, M., Geller, M. J., & Huchra, J. P. 1986, *AJ* 91, 1267
- Postman, M., Huchra, J. P., & Geller, M. J. 1986, *AJ* 92, 1238
- Postman, M., Geller, M. J., & Huchra, J. P. 1988, *AJ* 95, 267
- Postman, M., Huchra, J. P., & Geller, M. J. 1992, *ApJ* 384, 404
- Sandage, A. 1975, *Stars and Stellar Systems: Galaxies and the Universe*, University of Chicago Press
- Sargent, W, & Turner, E. 1977, *ApJ* 212, L3
- Scaramella, R., Baiesi-Pillastrini, G., Chincarini, G., Vettolani, G., & Zamorani, G. 1989, *Nature* 338, 562.
- Shectman, S.A., et al. 1996, *ApJ*, 470, 172
- Slingsend, K. A., 1996, University of Maine, PhD. dissertation.

- Slinglend, K., Batuski, D., Balkowski, C., & Olowin, R. 1995, in *Clustering in the Universe*, ed. S. Maurogordato et al. (Gif-sur-Yvette:Editions Fronteires), 261
- Slinglend, K., Batuski, D., Miller, C.M., Haase, S., Michaud, K., & Hill, J.M. 1998, *ApJS*, 115, 1
- Small, T., Ma, C.-P., Sargent, W., & Hamilton, D. 1998, *ApJ* 492, 45
- Smoot, G. F., Bennett, C. L., Kogut, A., et al. 1992, *ApJ* 396, L1
- Soneira, R. M., & Peebles, P. J. E. 1991, *AJ* 83, 845
- Struble, M. F., & Rood H. J. 1991, *ApJ* 374, 395
- Struble, M. F., & Rood H. J. 1991, *ApJS* 77, 363
- Sutherland, W. 1988, *MNRAS*, 234, 159
- Sutherland, W. & Efstathiou, G. 1991, *MNRAS*, 248, 159
- Tarenghi, M., Tifft, W. G., Chincarini, G., Rood, H. J., & Thompson, L. A. 1979, *ApJ*, 234, 793
- Tifft, W. G., & Gregory, S. A. 1988, *AJ* 95, 651
- Tonry, J., & Davis, M., 1979, *AJ* 84, 1511
- Tully, R. B. 1982, *ApJ*, 257, 389
- Tully, R. B. 1987, *ApJ* 323, 1
- Tully, R. B., Scaramella, R., Vettolani, G., & Zamorani, G. 1992, *ApJ* 388, 9
- Wagner, R. M., & Perrenod, S. C., 1981, *ApJ* 251, 424
- Yahil, A., Sandage, A., & Tammann G. A. 1980, *ApJ* 242, 448

Zabludoff, A., Huchra, J., & Geller, M., 1990, *ApJS* 74, 1

Zucca, E., Zamorani, G., Scaramella, R., & Vettolani, G., 1993, *ApJ* 407, 470

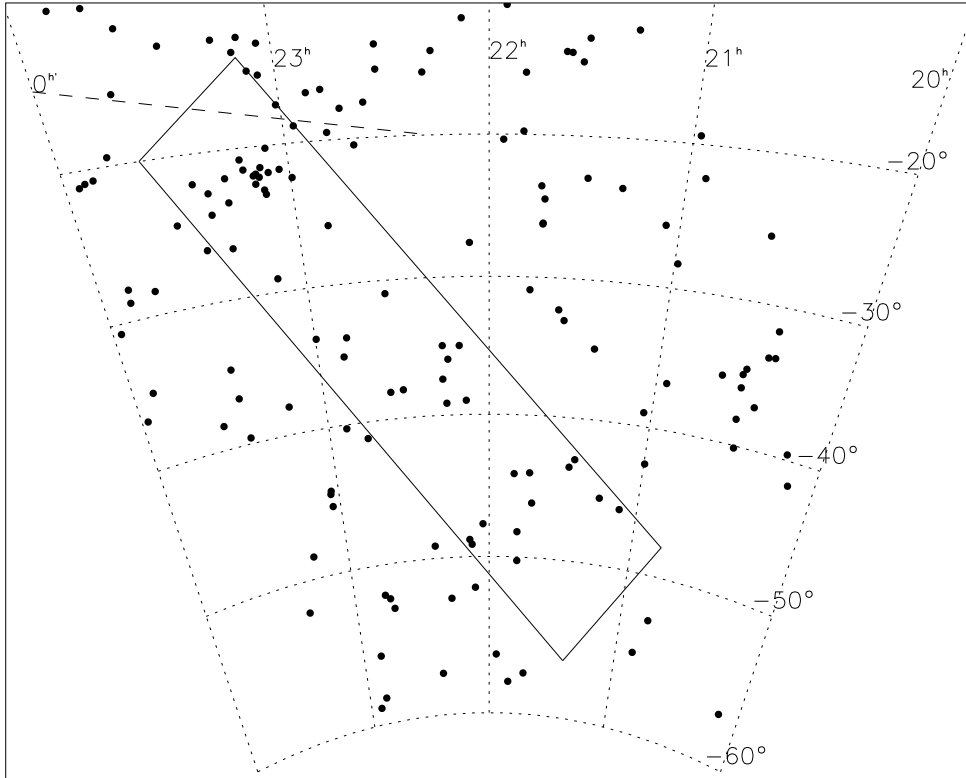


Fig. 1.— A gnomonic projection plot of the $R \geq 1$ ACO clusters with $m_{10} \leq 18.3$ in the general region of the sky of the strip (outlined by box) containing the two supercluster candidates targeted for the observations. North of $\delta = -17^\circ$ in this plot, the clusters are $R \geq 1$ Abell (1958) clusters and are limited to $z \leq 0.15$ (measured or estimated), approximately the estimated redshift of an $m_{10} \leq 18.3$ ACO cluster.

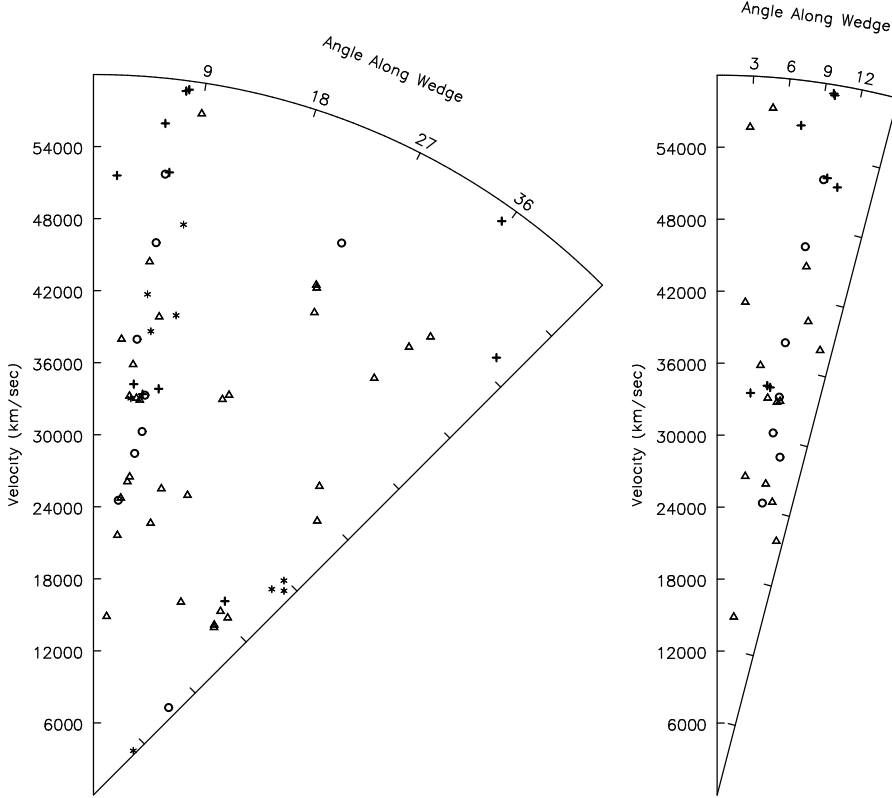


Fig. 2.— The left wedge plot shows Abell/ACO $R \geq 0$ cluster positions. The plot is 45° along our observed slice of sky by 10° in width (out of the page). Triangles in this figure represent $R \geq 1$ clusters with $m_{10} \leq 18.3$ and measured redshifts, which are 87% complete in the slice. The crosses are a few fainter $R \geq 1$ clusters, and the asterisks represent the $R = 0$ clusters with measured redshifts in this region. The right plot is the edge-on view of the left wedge, centered on the Aquarius filament and 10° in depth (out of page). This plot includes only $R \geq 1$ clusters, and is 95% complete in redshift coverage to $m_{10} = 18.3$. The Aquarius supercluster is centered roughly on $\alpha = 23^h 18^m$ and $\delta = -22^\circ$.

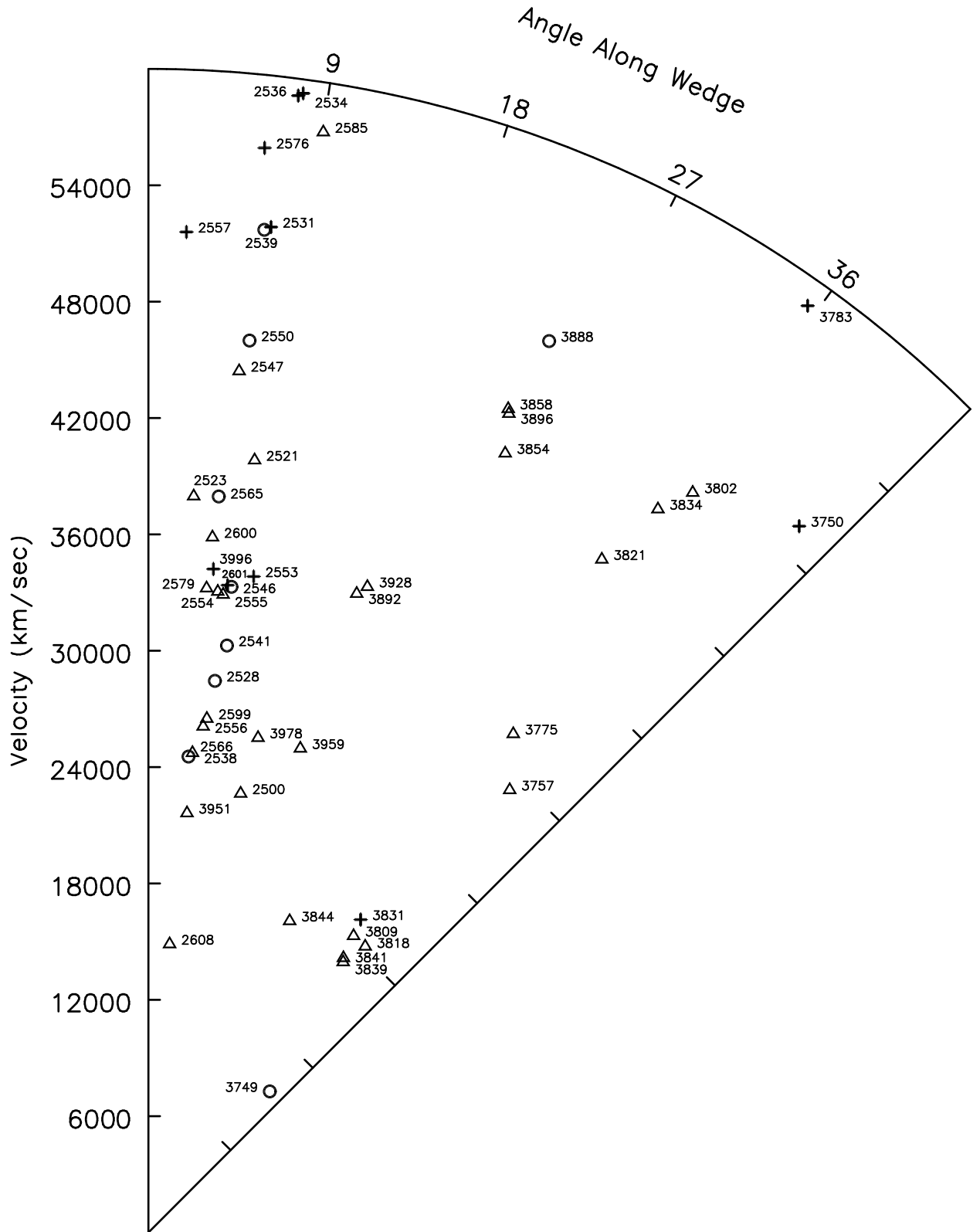


Fig. 3.— Similar to Fig. 2 (left), with Abell/ACO cluster catalog numbers shown. This plot contains only $R \geq 1$ clusters.

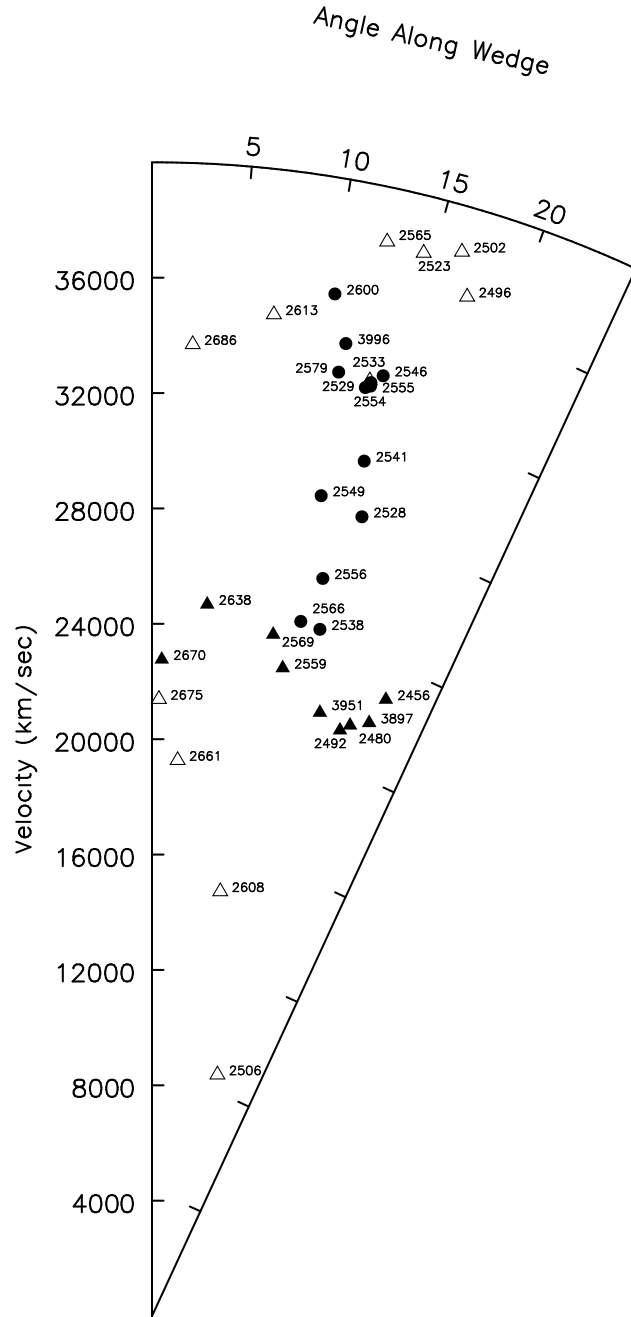


Fig. 4.— The centerline for this 25° by 12° wedge is traced by the dashed line in Fig. 1. The filled symbols represent clusters in the two large superclusters in this region that percolate at $n = 8\bar{n}$. Filled triangles represent members of Aquarius-Cetus, and filled circles represent those clusters in the Aquarius filament. Open triangles stand for clusters that did not percolate into either of these two superclusters at $n = 8\bar{n}$.

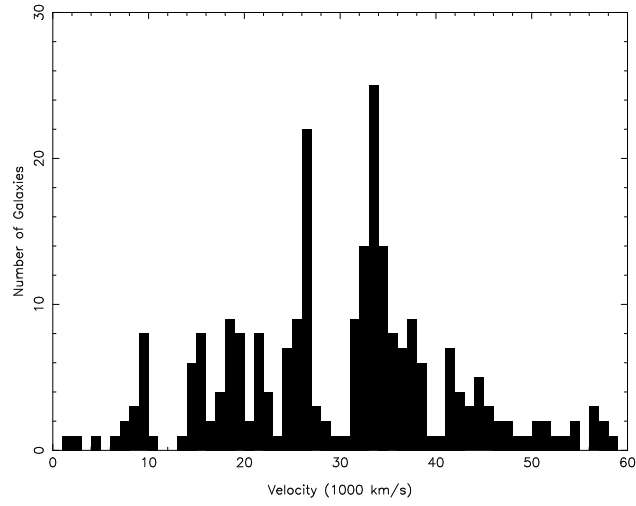


Fig. 5.— Histogram of the velocity distribution of 256 galaxies observed in all 17 cluster fields observed with MEFOS in the direction of the Aquarius supercluster candidate.

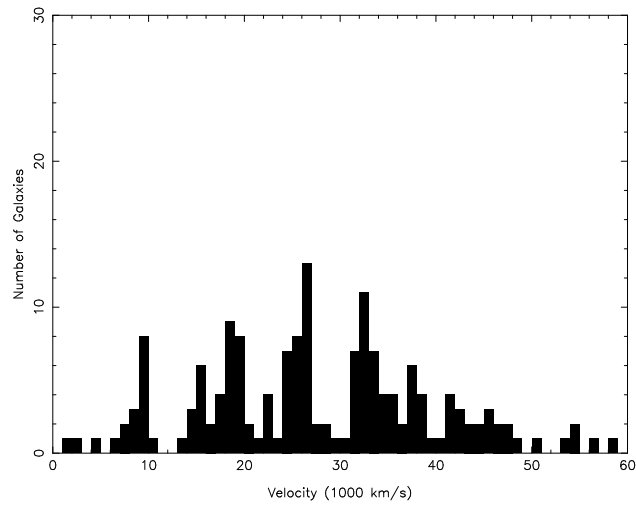


Fig. 6.— Histogram of the velocities from the same fields as in Fig. 5, but with galaxies identified as members of the Abell/ACO clusters in each observed field subtracted from the sample, leaving 169 galaxy velocities.

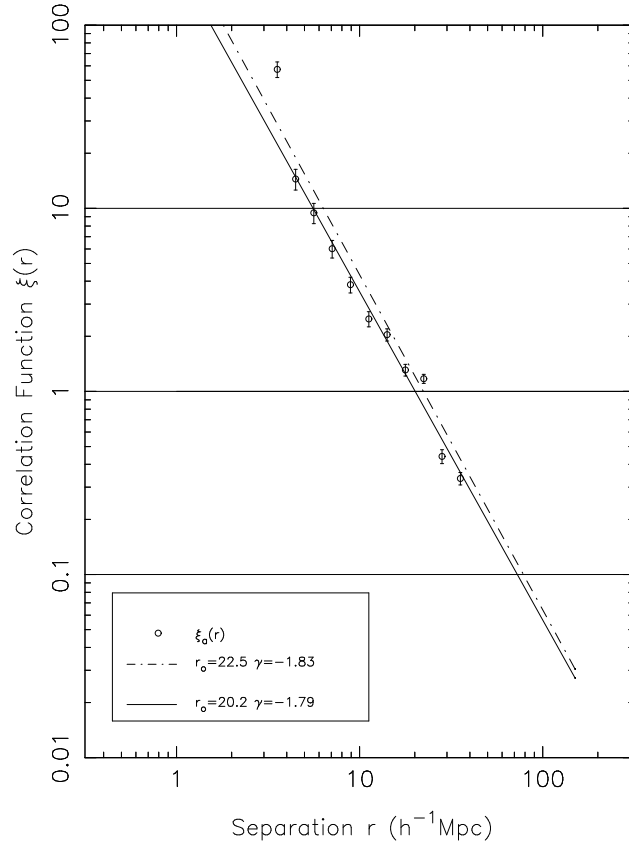


Fig. 7.— The two-point correlation function of a single simulated universe with cluster positions determined by Equation (3) (solid line), compared with the correlation function of Abell clusters (dash-dot line) from Miller et al. (1998).